

Durham Research Online

Deposited in DRO:

12 April 2013

Version of attached file:

Accepted Version

Peer-review status of attached file:

Peer-reviewed

Citation for published item:

Harvey, J. and Dale, C.W. and Gannoun, A. and Burton, K.W. (2011) 'Osmium mass balance in peridotite and the effects of mantle-derived sulphides on basalt petrogenesis.', *Geochimica et Cosmochimica Acta*, 75 (19). pp. 5574-5596.

Further information on publisher's website:

<http://dx.doi.org/10.1016/j.gca.2011.07.001>

Publisher's copyright statement:

NOTICE: this is the author's version of a work that was accepted for publication in *Geochimica et Cosmochimica Acta*. Changes resulting from the publishing process, such as peer review, editing, corrections, structural formatting, and other quality control mechanisms may not be reflected in this document. Changes may have been made to this work since it was submitted for publication. A definitive version was subsequently published in *Geochimica et Cosmochimica Acta*, 75 (19), 2011, 10.1016/j.gca.2011.07.001

Additional information:

Use policy

The full-text may be used and/or reproduced, and given to third parties in any format or medium, without prior permission or charge, for personal research or study, educational, or not-for-profit purposes provided that:

- a full bibliographic reference is made to the original source
- a [link](#) is made to the metadata record in DRO
- the full-text is not changed in any way

The full-text must not be sold in any format or medium without the formal permission of the copyright holders.

Please consult the [full DRO policy](#) for further details.

**OSMIUM MASS BALANCE IN PERIDOTITE AND THE EFFECTS OF
MANTLE-DERIVED SULFIDES ON BASALT PETROGENESIS**

J. Harvey^{1,2*}, C.W. Dale³, A. Gannoun^{1,4}, K.W. Burton,^{1,3,5}

¹ Dept. of Earth & Environmental Sciences, The Open University, Milton Keynes, UK.

² Current address, School of Earth & Environment, University of Leeds, UK.

³ Dept. of Earth Sciences, Durham University, UK.

⁴ Laboratoire des Magmas et Volcans, Université Blaise Pascal, Clermont-Ferrand, France.

⁵ Dept. of Earth Sciences, University of Oxford, UK.

* Corresponding author: email j.harvey@open.ac.uk / feejh@leeds.ac.uk

ABSTRACT

Analyses of enriched mantle (EM)-basalts, using lithophile element-based isotope systems, have long provided evidence for discrete mantle reservoirs with variable composition. Upon partial melting, the mantle reservoir imparts its isotopic fingerprint upon the partial melt produced. However, it has increasingly been recognised that it may not be simple to delimit these previously well-defined mantle reservoirs; the “mantle zoo” may contain more reservoirs than previously envisaged.

However, here we demonstrate that a simple model with varying contributions from two populations of compositionally distinct mantle sulfides can readily account for the observed heterogeneities in Os isotope systematics of such basalts without additional mantle reservoirs. Osmium elemental and isotopic analyses of individual sulfide grains separated from spinel lherzolites from Kilbourne Hole, New Mexico, USA demonstrate that two discrete populations of mantle sulfide exist in terms of both Re-Os systematics and textural relationship with co-existing silicates. One population, with a rounded morphology, is preserved in silicate grains and typically possesses high [Os] and low [Re] with unradiogenic, typically sub-chondritic $^{187}\text{Os}/^{188}\text{Os}$ attributable to long term isolation in a low-Re environment. By contrast, irregular-shaped sulfides, preserved along silicate grain boundaries, possess low [Os], higher [Re] and a wider range of, but generally supra-chondritic $^{187}\text{Os}/^{188}\text{Os}$ ([Os] typically $\leq 1\text{-}2$ ppm, $^{187}\text{Os}/^{188}\text{Os} \leq 0.3729$; this study). This population is thought to represent metasomatic sulfide.

Uncontaminated silicate phases contain negligible Os (<100 ppt) therefore the Os elemental and isotope composition of basalts is dominated by volumetrically insignificant sulfide ([Os] ≤ 37 ppm; this study). During the early stages of partial melting, supra-chondritic interstitial sulfides are mobilized and incorporated into the melt, adding their radiogenic $^{187}\text{Os}/^{188}\text{Os}$ signature. Only when sulfides armoured within silicates are exposed to

the melt through continued partial melting will enclosed sulfides add their high [Os] and unradiogenic $^{187}\text{Os}/^{188}\text{Os}$ to the aggregate melt. Platinum-group element data for whole rocks are also consistent with this scenario. The sequence of (i) addition of all of the metasomatic sulfide, followed by (ii) the incorporation of small amounts of armoured sulfide can thus account for the range of both [Os] and $^{187}\text{Os}/^{188}\text{Os}$ of EM-basalts worldwide without the need for contributions from additional silicate mantle reservoirs.

1. INTRODUCTION

Peridotite xenoliths are frequently entrained during the eruption of intra-plate magmas. Their utility in investigating mantle composition (e.g. Frey & Green, 1974; Ionov et al., 1993; Wilshire & Shervais, 1975; Stosch & Seck, 1980; Coisy & Nicolas, 1978; Stern et al., 1989) and basalt source reservoirs (e.g. Zindler & Hart, 1986; Hofmann, 1997) has been recognised for several decades. Their geographical dispersion is widespread and their accidental transport to the surface provides a means of sampling the mantle over a range of depths. Xenolith mineralogy, elemental composition, and isotope systematics all suggest that many peridotite xenolith suites have experienced varying degrees of partial melting (e.g. Jagoutz, et al., 1979; Galer & O’Nions, 1988) suggesting that suites of mantle xenoliths may be of particular utility in investigating the long term evolution and history of melt depletion in the mantle (e.g. Ross et al., 1954; Kuno & Aoki, 1970; Carlson & Irving, 1994; Pearson et al., 1995; Pearson, 1999; Griffin et al., 2003; Chu et al., 2009; Harvey et al., 2010).

Similarly, for several decades lithophile element-based isotope systems such as Sm-Nd, and Rb-Sr have been used to fingerprint the variable mantle sources (e.g. Galer & O’Nions, 1989) whose distinctive isotopic flavour is transferred to enriched-mantle (EM) basalts during partial melting. However, recent work involving the Re-Os isotope systematics of EM-basalts (e.g. Class et al., 2009) suggests that it may not be so simple to delimit these previously well defined mantle reservoirs; the “mantle zoo” (Stracke et al., 2005) may contain more reservoirs than previously envisaged. The commonly perceived understanding of how the Re-Os isotope system behaves during mantle melting is that the parent-daughter pair is unique due to the moderately incompatible and compatible nature of rhenium and osmium, respectively, on a bulk-rock scale (Pegram & Allègre, 1992); with rhenium, at least in part, residing within some silicate phases, e.g. garnet, based upon the observation that both Re and Yb concentrations are significantly higher in ocean island basalts (OIB) compared to

mid-ocean ridge basalts (MORB), i.e. $D^{\text{silicate/melt}} \approx Yb$ (Hauri & Hart, 1997; Righter et al., 1998). However, in detail, the bulk-rock budget of Re, Os and the other platinum group elements (PGE), and critically the behaviour of these elements during partial melting, is decoupled from the mechanisms that control lithophile element-based isotope systems. Osmium within the Re-Os isotope system and PGE abundance are controlled, in the main, by volumetrically minor (<0.03 modal %) sulfide (Luguet et al., 2003; 2004).

At least two populations of sulfide are commonly found within peridotite samples from the upper mantle. Sulfide grains wholly enclosed within silicate grains, and effectively shielded from interaction or re-equilibration with metasomatic agents, possess supra-chondritic IPGE (Os, Ir, Ru) abundances, lower PPGE (Pt, Pd, Rh) and Re abundances and often retain sub-chondritic Os isotope ratios attributable to their long-term isolation from the silicate melt from which they immiscibly separated (e.g. Alard et al., 2002, 2005; Griffin et al., 2004; Bockrath et al., 2005; Mungall & Su, 2005; Harvey et al., 2006, 2010). Interstitial, or intergranular sulfides possess supra-chondritic abundances of Re and PPGEs, lower IPGE (Os, Ir, Ru) abundances and variable (sub- to supra-chondritic) Os isotope ratios, (e.g. Burton et al., 1999; Alard et al., 2002; Pearson et al., 2004; Bockrath et al., 2004; Mungall & Su, 2005; Harvey et al., 2006, 2010; Luguet et al., 2008). This population of sulfides has been demonstrated to be highly mobile during metasomatic events (e.g. Harvey et al., 2010), being easily mobilized and redistributed by transient melts and fluids. Hence, in the specific context of PGE distribution between these populations of sulfide and their Re-Os isotope characteristics the sub-oceanic and subcontinental lithospheric mantle (SCLM) are very similar (cf. Alard et al. 2005; Harvey et al., 2006; Liu et al. 2008; Luguet et al. 2008 for sub-oceanic lithospheric mantle and e.g. Burton et al., 1999; Alard et al. 2002; Harvey et al. 2010 for SCLM). It is also the early mobilization of interstitial sulfides during the onset of partial melting to which the apparent “isotopic gap” between mid-oceanic ridge basalts (e.g.,

Gannoun et al., 2004, 2007; Escrig et al., 2005), oceanic basalts (Reisberg et al., 1993; Roy-Barman & Allègre, 1995; Luguet et al., 2008) and abyssal peridotites (e.g., Alard et al., 2005; Harvey et al., 2006; Liu et al., 2008) has been attributed; a process that may also occur in SCLM settings and go at least some way to explaining the notoriously difficult interpretation of bulk rock rhenium-depletion (T_{RD}) ages (Rudnick & Walker, 2009).

This study presents bulk-rock PGE abundances and Re-Os elemental and isotope analyses of bulk-rock, silicate and spinel mineral separates, and 2 populations of sulfide in a suite of 28 peridotite xenoliths from Kilbourne Hole, New Mexico, USA. We demonstrate that the behaviour of the two compositionally and texturally distinct populations of peridotite-hosted sulfide controls the behaviour of Re and Os during partial melting. Moreover, using a simple two-stage model we demonstrate a means for the generation of the range of Re-Os elemental and isotopic compositions of worldwide EM-basalts without the need of additional mantle reservoirs to those proposed by Zindler & Hart (1986) and Hofmann (1997).

2. GEOLOGICAL SETTING, PETROLOGY AND PETROGRAPHY OF SAMPLES

Kilbourne Hole is one of several late Pleistocene volcanic maars situated in the Potrillo volcanic field on the axis of the Rio Grande Rift, an asymmetric system of grabens which extends for over 1000 km north – south through Colorado, New Mexico and Texas in the USA and onwards into Chihuahua, northern Mexico. The petrology and petrography of Kilbourne Hole mantle xenoliths have been the subject of extensive prior study, (e.g. Carter, 1965; Reid & Woods, 1978; Irving, 1979, 1980; Basaltic Volcanism Study Project, 1981; Bussod, 1981; Bussod & Irving, 1981). Mantle and crustal xenoliths are abundant in the lava flows in the Kilbourne Hole area. Dates for the eruption of the host basanite range from $80 \text{ Ka} \pm 10 \text{ Ka}$ (Bussod & Williams, 1991; Thompson et al., 2005) to $141 \text{ Ka} \pm 75 \text{ Ka}$ (Hoffer, 1976; Dromgoole & Pasteris, 1987) which suggests that any xenoliths exhumed at Kilbourne Hole have been separated from their source for only a relatively short period of geological time and are thus representative of the present-day mantle underlying the south-western USA.

The samples examined during the course of this study ($n = 28$) are Cr-diopside spinel lherzolites and spinel harzburgites with protogranular textures. A single sample (KH03-21) has a texture transitional between protogranular and porphyroclastic. Grain size is therefore generally greater than 1 mm and the samples are almost exclusively coarse grained. Porphyroclastic and granular xenoliths have also been reported at Kilbourne Hole. Although other petrographic textures have been observed (mosaic-porphyroclastic, tabular granular; Dromgoole & Pasteris, 1987; Kil & Wendlandt, 2004) textures other than protogranular are in fact rare at this locality and protogranular xenoliths are most representative of those recovered from Kilbourne Hole (Kil & Wendlandt, 2004).

Large ($>1 \text{ kg}$) xenoliths were preferentially selected so that host basalt could be trimmed and the possible effects of host infiltration minimised while still retaining sufficient

material (>500 g) to represent a homogenous sample at the bulk-rock scale. The samples for this study were also selected so as to represent a wide range of clinopyroxene modal abundance, estimated visually in the field and subsequently calculated using a least squares regression method (Tarantola & Valette, 1982). Chrome-diopside modal abundance ranges from 3.3% to 17.2% (± 1.6). No discrete metasomatic phases (e.g. phlogopite, amphibole, apatite) were detected during this study, or any prior study of this locality.

In addition to the silicate phases and spinel, which account for in excess of 99.97% of the volume of the samples, individual sulfide grains ($n = 33$) with bulk compositions broadly equivalent to pentlandite-rich and pentlandite-poor monosulfide solid solution (Luguet et al., 2003, 2004) were also analysed for major element abundances, Os abundances and Os isotopes.

3. ANALYTICAL METHODS

Samples were cut and washed to remove host basalt, surface alteration and contamination and rinsed in ultra-pure ($>18\text{ M}\Omega$ reverse osmosis scrubbed) water. Samples selected for bulk-rock analysis were dried and then powdered in an agate mortar. For the bulk-rock Re-Os measurements $\sim 2\text{ g}$ of peridotite was dissolved in inverse aqua regia (3 mL 12M HCl / 9 mL 16M HNO_3) in sealed Carius tubes at 230°C for 7 days (Shirey & Walker, 1995). A spike solution, enriched in ^{185}Re and ^{190}Os , was added immediately before the addition of the acids. Osmium was purified using CCl_4 , leaving Re in the inverse aqua regia fraction (Cohen & Waters, 1996). The Os was subsequently recovered from the CCl_4 in HBr, microdistilled for 3 h at 90°C (Birck et al., 1997) and dried down. Rhenium was extracted by drying down the inverse aqua regia and redissolving the residue in 2M Teflon-distilled HNO_3 . The Re was recovered in iso-amylol (Birck et al., 1997), cleaned in a wash of 2M HNO_3 and finally extracted in ultrapure water. The reference material UB-N, a serpentinised peridotite, was digested numerous times ($n = 6$) to assess the efficacy of the Carius tube dissolution method for bulk-rock peridotite. Meisel et al. (2003) questioned “traditional” methods (i.e. low temperature acid attack; Carius tubes) for peridotite dissolution, citing resistant phases remaining undissolved which, in turn, led to poor reproducibility of Os concentrations and Os isotope ratios. Osmium concentrations of UB-N (3.4 to 4.2 ppb, $n = 6$) were indistinguishable from those obtained by high-pressure asher (e.g. Meisel et al., 2003), although the values obtained for the Os isotope ratio of UB-N were somewhat variable ($^{187}\text{Os}/^{188}\text{Os} = 0.1250 \pm 2$ to 0.1279 ± 1). However, repeat digestions of Kilbourne Hole bulk-rock samples (KH03-6, KH03-21 & KH03-25) by Carius tubes performed during this study demonstrate excellent reproducibility for both osmium concentrations and Os isotope ratios (e.g. KH03-06: $[\text{Os}] = 1.54 \pm 0.10$ (2 sd); $^{187}\text{Os}/^{188}\text{Os} = 0.1269 \pm 4$ (2sd); $n = 4$). This suggests that the variability in the Os isotope measurements for UB-N obtained during this

study are more likely attributable to heterogeneity in the reference material, i.e. a nugget effect at the 2 g sample size, rather than artefacts attributable to incomplete digestion. Notwithstanding the possibility of either incomplete digestion or a nugget effect in the analysis of UB-N, neither of these factors appear to affect repeat analyses of Kilbourne Hole xenoliths. Reproducibility of Re concentrations in duplicate analyses is comparable to that achieved on corresponding Os measurements (KH03-21 [Re] = 0.08 ± 0.3 (2 s.d.) $n = 4$; KH03-10 [Re] = 0.23 ± 0.10 (2 s.d.) $n = 2$; KH03-6 [Re] = 0.07 ± 0.02 (2 s.d.) $n = 4$). Repeat digestions of reference material UB-N ($n = 6$) yielded Re concentrations of 0.184 ± 0.071 ppb, slightly below the preferred value of Meisel et al. (2003) which ranges from 0.201 to 0.241 ppb, although as stated above this likely reflects the heterogeneity of the reference material rather than inaccuracy of the measured concentration of a particular digestion. Reproducibility of Os isotope ratios in Kilbourne Hole bulk-rock peridotites is good. For example, repeat analyses of KH03-6 ($n = 4$) and KH03-21 ($n = 3$) differed by 0.14 % and 0.09 % respectively. Total procedural blanks for bulk-rock Os measurements during the course of this study were 3.85 ± 3.0 pg, $^{187}\text{Os}/^{188}\text{Os} = 0.170 \pm 0.031$, and for Re 1.85 ± 2.15 pg.

Aggregates of optically pure olivine, orthopyroxene, clinopyroxene and spinel were handpicked under a binocular microscope to ensure that both visible inclusions and surficial adherents were absent. The aggregates were repeatedly rinsed in analytical grade acetone and ultra-pure water before being powdered in an agate pestle and mortar. The powdered aggregates were then digested and Os and Re purified and recovered by low temperature acid attack, closely following the method described by Birck et al. (1997) and previously employed by Burton et al. (1999) and Harvey et al. (2010) on mineral phases from similar xenolithic material.

Rhenium–osmium chemistry for individual hand-picked sulfide grains was achieved using a modified microdistillation technique that closely follows previously reported procedures (Pearson et al., 1998). The total procedural blanks for Os in individual sulfides were 0.10 ± 0.06 pg, $^{187}\text{Os}/^{188}\text{Os} = 0.36 \pm 0.50$, and for Re 3.14 ± 0.61 pg. Both Re and Os samples were analysed on platinum filaments using negative thermal ionisation mass spectrometry (N-TIMS) (Volkening et al., 1991; Creaser et al., 1991) using a ThermoScientific Triton at The Open University, collecting individual masses by peak jumping on a secondary electron multiplier. Long term accuracy of a Johnson Matthey standard solution (14 pg to 8 ng; $n = 85$) is generally within 0.1% of the recommended values for $^{187}\text{Os}/^{188}\text{Os}$. Typical signal intensities of ^{190}Os were in excess of 250,000 cps.

Bulk-rock PGE abundances of 6 peridotite xenoliths and the host basalt were determined using the anion-exchange column procedures of Pearson & Woodland (2000) and Dale et al. (2008). Bulk-rock powders were digested, together with a mixed PGE spike, in inverse aqua regia (2.5 mL 12M HCl, 5 mL 16M HNO_3) in an Anton Paar high-pressure asher. Following Os extraction by CCl_4 , the inverse aqua regia was dried, refluxed in 12M HCl and dried again. Chrome in its oxidised form (Cr^{6+}) can be present after aqua regia digestion and behaves similarly to PGE on the anion exchange resin and hence can be eluted with the PGE, causing polyatomic isobaric interferences on isotopes of Ru (Meisel et al., 2008). Therefore, any Cr^{6+} present was reduced by the addition of H_2O_2 , which was then dried and the residue taken up in 10 mL of 0.5M HCl and loaded onto a column containing AG1X-8 (100–200#) anion-exchange resin. The sample matrix was eluted with 10 mL of 1M HF/1M HCl and 0.8M HNO_3 before Ir, Ru, Pt and Re were collected in 10 mL of 13.5M HNO_3 . Palladium was collected in 20 mL of 9M HCl after further elution of Zr using 1M HF/1M HCl. Both the Ir–Pt–Ru–Re and the Pd cuts were dried down and taken up in 1 mL of 0.5M HCl for analysis using the ThermoScientific Element2 ICP-MS at Durham University.

Details of mass spectrometry procedures are given in Dale et al. (2008). The reproducibility of Ir, Pt and Pd abundances in the peridotite reference material GP13 is ~10% RSD, whereas Re has an uncertainty of 3% RSD. Reproducibility of IPGE, based upon multiple Os analyses of the peridotite samples is a maximum of $\pm 6\%$ (2σ).

4. RESULTS

4.1 Bulk rock Re and Os elemental and isotope measurements.

Bulk-rock Re concentrations ([Re]) range from 0.007 ppb to 0.693 ppb, with a mean concentration of 0.094 ppb (Table 1). The range of [Re] obtained during this study is much larger than that of Meisel et al. (2001) whose whole rock [Re] of samples from the same locality range from 0.053 ppb to 0.432 ppb. The mean [Re] from this study, like the mean Os concentration ([Os]), is significantly lower than the average mantle composition of 0.35 ppb (Becker et al., 2006) (Figure 1). Bulk-rock [Os] from this study (0.802 to 3.544 ppb, mean = 1.828; Table 1) are similar to previous studies of this locality (Morgan, 1986; Burton et al., 1999; Meisel et al., 2001) and studies of other peridotite suites from similar non-cratonic settings (e.g. Alard, 2002; Meisel et al., 2001; Liu et al., 2008; Ackerman et al., 2009; Harvey et al., 2010; Wittig et al., 2010) but are significantly lower than the mantle average (Becker et al., 2006).

The bulk-rock $^{187}\text{Os}/^{188}\text{Os}$ ratios of the samples range from 0.1159 to 0.1339 with a mean of 0.1256 (Table 1). All but 3 of the 28 xenoliths analysed have $^{187}\text{Os}/^{188}\text{Os}$ ratios < 0.1296 , the maximum present day estimate of the primitive upper mantle (PUM) of Meisel et al. (1996; 2001) and more than two thirds of the samples ($n = 23$) have sub-chondritic $^{187}\text{Os}/^{188}\text{Os}$ i.e. < 0.1270 (Walker & Morgan, 1989; Luck & Allègre, 1993). The values obtained in this study are similar to those from previous studies of this locality (Burton et al., 1999; Meisel et al., 2001) i.e. $^{187}\text{Os}/^{188}\text{Os} = 0.117$ to 0.130 , mean 0.1257 , ($n = 17$). Whole rock $^{187}\text{Re}/^{188}\text{Os}$ ratios range from 0.009 to 1.35 with a mean of 0.222. However, only 3 samples, KH96-8, KH96-20 and KH96-24, have suprachondritic ratios (i.e. > 0.4) and excluding these 3 samples gives a much narrower range of $^{187}\text{Re}/^{188}\text{Os}$ ratios (0.009 to 0.306,

mean = 0.156). This differs somewhat from previous work on xenoliths from the same locality (Burton et al., 1999; Meisel et al., 2001) where the range of $^{187}\text{Re}/^{188}\text{Os}$ values was 0.228 to 0.781 and the mean much higher (0.395), i.e. near chondritic.

Figure 2a is a Re-Os isotope evolution diagram for the 28 bulk-rock peridotites from this study. There is a broad positive co-variation between $^{187}\text{Re}/^{188}\text{Os}$ and $^{187}\text{Os}/^{188}\text{Os}$ and the best fit line coincides with a calculated isochron age of 2.3 ± 0.7 Ga, but the relationship cannot be described as convincingly isochronous despite, superficially at least, being in good agreement with the ages derived from Sr isotope ratios of Roden et al. (1988) of $2.5 \text{ Ga} \pm 0.2$ Ga for the SCLM beneath the south-western USA. On a bulk-rock scale Re has been described as a moderately incompatible element during partial melting, contrasting with the compatible bulk-rock behaviour of Os during melt depletion (Hart & Ravizza, 1996). However, Re is mobile under a wide range of conditions (Meisel et al., 1996, 2001; Sun et al., 2004), and the large degree of scatter on bulk-rock Re-Os isotope evolution diagrams can be attributed, at least in part, to rhenium mobility. The best fit line in Figure 2a does not pass through the estimated composition for PUM (Meisel et al., 2001) and the suite of samples from this study appears displaced to a lower $^{187}\text{Re}/^{188}\text{Os}$ composition than those of Meisel et al. (2001) supporting the notion that bulk rock Re may not behave in a systematic manner and may be heterogeneous over spatially restricted areas.

A number of proxies for $^{187}\text{Re}/^{188}\text{Os}$ have therefore been sought amongst elements that are not only moderately incompatible but also immobile and unaffected by secondary processes not related to melt depletion. For example, Al, S and Yb (Reisberg et al., 2005; Hauri & Hart, 1997; Burnham et al., 1998 respectively) are all believed to have similar bulk partition coefficients to Re during partial melting but are generally considered to be immobile at sub-magma generating temperatures. Figure 2b illustrates a much reduced degree of scattering ($R^2 = 0.89$) between $^{187}\text{Os}/^{188}\text{Os}$ and Al_2O_3 and yields an “aluminachron” age

(Reisberg & Lorand, 1995) of 2.4 Ga, in good agreement with the best fit line through the Re-Os isotope evolution diagram in Figure 2a and the Sr isotope age of Roden et al. (1988). We expand on the subject of Re mobility below in the discussion of metasomatic sulfides and their mobility.

4.2 Bulk-rock PGE measurements

Six peridotite xenoliths (KH03-10, KH03-15, KH03-16, KH03-18, KH03-21 & KH03-24) that have experienced a wide range of melt depletion (1.1 to 4.4 wt.% bulk-rock Al_2O_3) were selected for bulk-rock platinum-group element (PGE) measurements. In addition, PGE abundances were also obtained for the host basalt. Bulk-rock PGE abundances (Figure 3) are similar to those obtained elsewhere for non-cratonic lherzolites and harzburgites (e.g. Lorand & Alard, 2001; Lorand et al., 2003; Wittig et al., 2010) but also overlap with the lower end of PGE concentrations obtained from bulk-rock cratonic peridotites (e.g. Pearson et al., 2004; Ivanov et al., 2008), orogenic massifs (e.g. van Acken et al., 2010) and ophiolitic peridotite (Hanghøj et al., 2010). Osmium, iridium and ruthenium (IPGE) abundances vary comparatively little within the samples analysed ($[\text{Os}] = 1.39$ to 3.36 ppb; $[\text{Ir}] = 2.81$ to 4.19 ppb; $[\text{Ru}] = 4.77$ to 7.47 ppb; Table 4) whereas Pt and Pd (PPGE), along with Re, show much greater variability in elemental abundance ($[\text{Pt}] = 3.35$ to 6.58 ppb; $[\text{Pd}] = 0.55$ to 5.58 ppb; $[\text{Re}] = 0.002$ to 0.265 ppb; Table 4). While there is no strong co-variation between indices of melt depletion (e.g. bulk-rock MgO or Al_2O_3) and PGE abundance the more fertile peridotites do tend to contain higher abundances of PPGE than less fertile samples, i.e. the fractionation of IPGE from PPGE appears, in general, to be most pronounced in the most depleted peridotites, with Re being the most strongly fractionated from the IPGEs.

4.3 Re-Os abundance and isotope ratios of silicate minerals and spinel

Optically pure mineral separates of olivine, orthopyroxene and clinopyroxene, spinel and individual sulfide grains were handpicked from 4 xenoliths, KH03-15, KH03-16, KH03-21 and KH03-24. These samples were selected on the basis of their wide range of modal abundance of clinopyroxene (2.5 to 17.5 modal %). Osmium concentrations of the silicate phases are presented in Table 2. The high [Os] of clinopyroxene from KH03-16 is probably derived from contamination from one or more microscopic sulfide grains enclosed within the clinopyroxene (surficial contamination, if unobservable during the picking, would probably have been removed during the cleaning process). Osmium concentrations in spinel are up to an order of magnitude more Os than many of the co-existing silicate phases. It is difficult to assess the origin of the high [Os] of spinel as its opaque nature makes it impossible to guarantee that handpicked grains are free from sulfide inclusions. With the exception of presumably contaminated clinopyroxene from KH03-16, [Os] increases in the following manner: olivine < orthopyroxene < clinopyroxene < spinel.

Rhenium concentrations of the same silicates are also presented in Table 2. Spinel tends to have higher [Re] than the silicate phases (47.1 ppt to 818 ppt) (Table 2). While spinel invariably contains the greatest [Re], the distribution of Re amongst the silicate phases is not as clear as the relationship shown for [Os] above. Olivine has the lowest [Re] in all 4 of the samples and the two pyroxenes have a lower [Re] than spinel (other than clinopyroxene from KH03-16, which may be contaminated by sulfide). Although the experimental results of Mallmann & O'Neill (2007) and Righter et al. (2004) suggest that Re does partition into clinopyroxene to a certain extent, the relative partitioning of Re between the pyroxenes in this study is not systematic. The Os isotope ratios and $^{187}\text{Re}/^{188}\text{Os}$ ratios for silicate mineral

separates are presented in Table 2. In all cases Os isotope ratios of mineral separates are higher than the corresponding bulk-rock values. Because of the large uncertainties on the mineral Re-Os isochrons no meaningful age information is preserved in the silicate phases alone.

The presence of contamination from included sulfide grains in clinopyroxene from KH03-16 raises the question of whether all of the [Re] and [Os] for mineral separates from this study can be accounted for by varying degrees of sulfide contamination. Burton et al. (1999) demonstrated the effect of included sulfides upon the Os elemental and isotope ratio of a mineral separate. In their study, minerals with sulfide contamination have elevated [Os] (an order of magnitude greater than their clean mineral separates) and Os isotope ratios were indistinguishable from the bulk-rock value. Osmium concentrations of clean mineral separates from this study are similar to those obtained by Burton et al. (1999). The probability of the same degree of sulfide contamination in mineral separates from independent studies is very small. Similarly, the sequential increase in concentration from olivine, through orthopyroxene and clinopyroxene to spinel from all 4 samples from this study (with the exception of KH03-16 clinopyroxene) is difficult to account for with the [Os] being solely attributed to contamination from sulfide inclusions.

4.4. Major element abundances, Re-Os concentration and isotope systematics of individual sulfide grains.

4.4.1 Major element abundances of individual sulfide grains

Based upon the relative proportions of Ni, Fe and Cu, three populations of sulfide have been identified in the Kilbourne Hole xenoliths from this study (Figure 4). Two of the

populations have low Cu abundance (0.08 to 4.68 wt %) and are defined by either a high or low Fe:Ni ratio. Major element abundances of 57 sulfides derived by electron microprobe are given in Table 3. These two populations are broadly equivalent to pentlandite-rich and pentlandite-poor monosulfide solid solution (MSS) sulfides (Luguet et al., 2003, 2004). Within the MSS sulfides analysed there is a broad inverse co-variation between Ni and Fe abundances. The third population of sulfide is characterised by a significantly higher Cu abundance, analogous to chalcopyrite rich sulfides from previous studies (Dromgoole & Pasteris, 1987; Luguet et al., 2003, 2004).

High-Cu sulfides from this study have very high Fe:Ni ratios and plot significantly below the array of the monosulfide solid solution samples. The relative proportion of Ni, Fe, and Cu in sulfides has implications for the capacity of a sulfide to host Os. Monosulfide solid solution with higher Ni content has a greater proportion of octahedral sites in which Os is commonly hosted (Mackovicky et al., 1986; Cabri, 1999; Ballhaus et al., 1999). A single sulfide with a composition similar to that of the basalt hosted sulfide of Burton et al. (1999) is also illustrated in Figure 4. However, in this instance the sulfide is located within a peridotite xenolith (KH03-23) rather than the host basalt suggesting that some degree of infiltration of and interaction with the host lava itself has occurred (Hammond et al., 2010).

4.4.2. Re-Os concentration and isotope systematics of individual sulfide grains

Individual sulfide grains have by far the highest Os content of any of the constituent phases of mantle xenoliths. All of the xenoliths from which mineral separates were picked contain sulfides with [Os] several orders of magnitude greater than any of the co-existing silicates or spinel. A total of 33 individual sulfide grains were analysed: KH03-15 (n = 7), KH03-16 (n = 7), KH03-21 (n = 10) and KH03-24 (n = 9). Their [Os] vary from 0.001 ppm

to 36.85 ppm (Table 5). Rhenium concentrations of the sulfide grains are also high and, in general, orders of magnitude greater than the silicate phases and spinel. Rhenium concentrations for 19 sulfide grains were obtained during this study (KH03-15, n = 4; KH03-16, n = 5; KH03-21, n = 4; KH03-24, n = 6) which range from 0.002 ppm to 138.9 ppm (Figure 6). Curiously, sulfide grains from relatively fertile samples (KH03-21 and KH03-24) have a narrow range of [Os] but a wide range of [Re] and sulfide grains from depleted, metasomatised samples (KH03-15 and KH03-16) show the opposite i.e. a wide range of [Os] but a restricted range of [Re].

The morphology of each individual grain was assessed in an attempt to determine the textural location of the sulfide prior to disaggregation of the xenolith and hand-picking of the grain. The separated grains were categorised as either euhedral / rounded / subrounded, or anhedral / subhedral / irregular. The former were inferred to have originated as grains armoured within individual silicate grains while the latter were ascribed to an interstitial origin (Alard et al., 2002). Euhedral / rounded / subrounded grains tend to have high Os concentration and low Re concentrations while the converse is generally true in the anhedral / subhedral / irregular grains.

The 33 individual sulfide grains have Os isotope ratios ranging from 0.1185 to 0.3729. Sulfides from individual xenoliths also have a wide range of $^{187}\text{Os}/^{188}\text{Os}$ ratios (Table 5). Within the entire sulfide population there is a broad inverse trend between Os isotope ratio and [Os], i.e. grains with the highest [Os] are frequently the least radiogenic and *vice versa* (Figure 5). Although the trend as a whole is less clear in the bulk-rock measurements, Figure 5b illustrates that the samples with the highest bulk-rock [Os] also tend towards the lower Os isotope ratios. Enclosed sulfide grains, which are often rounded, subrounded or euhedral in shape, have uniformly low $^{187}\text{Os}/^{188}\text{Os}$ values that are slightly below or indistinguishable from the bulk-rock Os isotope ratio (Figure 5b) and commonly have the highest [Os] and low

[Re]. Interstitial sulfide grains are often anhedral, irregular or subangular shaped and, like the silicate and spinel mineral separates, are characterised by Os isotope ratios that exceed those of the corresponding bulk- rock value. They have much lower [Os] and higher [Re] than the other sulfide population. That the silicate minerals and interstitial sulfides in many cases yield similar Os isotope compositions for a range of Re/Os ratios suggests a degree of recently attained isotopic equilibrium (cf. Burton et al., 1999).

5. DISCUSSION

5.1. Bulk rock Re-Os isotope systematics during partial melting.

The commonly held perception of the behaviour of Re and Os on a bulk-rock scale is that Os behaves as a compatible element during partial melting of the mantle. This contrasts with Re which behaves as a moderately incompatible element (e.g. $D_{\text{Re}}^{\text{opx/melt}} = 0.013$, $D_{\text{Re}}^{\text{cpx/melt}} = 0.18\text{--}0.21$; Righter et al., 2004). A first order prediction therefore would be that this will result in a residue that, after melt extraction, retains a moderately high Os content yet is significantly depleted in Re; almost complete exhaustion of Re can be expected with continued melt depletion. In the absence of subsequent metasomatism, evidence for prior melt depletion should therefore be preserved within, for example, peridotite xenoliths and will be characterized by unradiogenic, i.e. sub-chondritic Os isotope ratios ($^{187}\text{Os}/^{188}\text{Os} < 0.1270$; Luck & Allègre 1983; Walker & Morgan, 1989). However, metasomatism occurring after melt depletion has the effect of obscuring the primary Os isotope signature of ancient melt depletion. This may take the form of addition of ^{187}Os from material recycled back into the asthenosphere or by adding metasomatic Re which, over time, will generate radiogenic ^{187}Os , thus shifting bulk-rock $^{187}\text{Os}/^{188}\text{Os}$ to higher values.

Conversely, enriched-mantle (EM) basalts produced by the partial melting of peridotite generally contain significantly less Os than peridotite (often < 10 ppt, average $[\text{Os}] = 428$ ppt; Reisberg et al., 1993; Roy-Barman & Allègre, 1995; Martin et al., 1994; Bennett et al., 1996; Hauri & Kurz, 1996; Hauri et al., 1996; Lassiter & Hauri, 1998; Widom et al., 1999; Brandon et al., 1999, 2007; Lassiter et al., 2000, 2003; Skovgaard et al., 2001; Eisele et al., 2002; Workmann et al., 2004; Gaffney et al., 2005; Jamais et al., 2008; Debaille et al., 2009; Day et al., 2009; Class et al., 2009), but occasionally extend to values comparable with those of peridotite samples (e.g. >4.4 ppb; Ireland et al., 2009). Although isolated EM-basalts

have relatively unradiogenic $^{187}\text{Os}/^{188}\text{Os}$ (e.g. as low as 0.1212; Debaille et al., 2009) in general EM-basalts have radiogenic Os isotope ratios, extending to $^{187}\text{Os}/^{188}\text{Os} = 0.2621$ (Ireland et al., 2009). All of these observations are consistent with, on a bulk-rock scale, Os behaving as a compatible element during partial melting and the moderately incompatible nature of Re. When plotted against a reliable index of melt depletion, e.g. bulk-rock Al_2O_3 wt%, peridotite Os isotope ratios seem to co-vary with the effects of the extraction of increasing amounts of basaltic melt (e.g. Reisberg & Lorand, 1995). Lower Os isotope ratios coupled with low Al_2O_3 wt% would seem consistent with the early and efficient removal of Re during melt depletion and a lack then of radiogenic ingrowth of ^{187}Os – a process masked in Figure 2a by the subsequent addition of metasomatic Re but seemingly stripped away by using a suitable proxy for melt depletion in Figure 2b.

However in detail, Os elemental abundances of, in particular, non-cratonic xenoliths such as those from this study, and other non-cratonic xenolith localities worldwide, are simply not consistent with the notion that on a bulk-rock scale Os behaves as a compatible element during partial melting. What is inconsistent with this hypothesis is that only 1 sample from this study and 3 samples in total, from 42 samples in 4 separate studies of this locality (Morgan, 1986; Burton et al., 1999; Meisel et al., 2001; this study) have [Os] that are higher than a nominally fertile mantle – a characteristic that should be the norm rather than the exception if Os behaves compatibly on a bulk-rock scale during partial melting. In effect, there is a significant deficiency of [Os] in bulk-rock peridotite if Os behaves in a compatible manner during melt depletion and if this is the main control on the behaviour of this element.

5.2 Osmium mass balance in peridotites

Several earlier studies (Hart & Ravizza, 1996; Burton et al., 1999; Harvey et al., 2010) have demonstrated that the contribution to the [Os] of bulk-rock peridotites derived from the major rock-forming minerals (olivine, orthopyroxene, clinopyroxene, spinel) is negligible. In optically pure hand-picked aggregates of these minerals from this study no more than 5% of bulk-rock Os can be accounted for from these phases. This is consistent with previous experimental studies (e.g. Fleet et al., 1991, 1996, Brenan et al., 2003, 2005) which determined the relative affinities of Os and the other PGE between sulfide and silicate assemblages. The experimentally derived partition coefficients for Os between sulfide and silicate liquids ($D_{Os}^{\text{sulfide/silicate}}$) of 10^4 to 10^6 are supported by the [Os] measured in optically pure silicate phases and hand-picked individual sulfide grains of this study (Table 5). Thus, volumetrically insignificant sulfides account for >95% of the Os mass balance of peridotite xenoliths. It is the behaviour of sulfide during melt depletion that will determine the Os abundance and isotope systematics of a basalt formed by the partial melting of a predominantly silicate pre-cursor source rock. However, compositional heterogeneity exists within mantle sulfide populations; Alard et al. (2002) and Pearson et al. (2002) identified two distinct sulfide populations based upon their morphology, [Os], $^{187}\text{Os}/^{188}\text{Os}$, [Re] and textural constraints. Sulfides that appear to be entirely enclosed within silicate grains, and thus protected from any subsequent interaction with melts or fluids tend to be rounded to sub-rounded, have high Os concentration ([Os] = 10s ppm), unradiogenic (sub-chondritic) $^{187}\text{Os}/^{188}\text{Os}$ and low [Re], thus reflecting a long term evolution in a low-Re environment and probably representing the separation of an immiscible sulfide liquid during a previous melt depletion event (e.g. Holzheid, 2010). This is consistent with the findings of Bockrath et al. (2004) and Mungall & Su (2005) where Os-Ir-Ru rich sulfides remained in a peridotite

635 residue because of their tendency to adhere to silicate grains. This also supports the notion
636 that enclosed sulfides are the result of an immiscible sulfide liquid that separated from a co-
637 existing silicate liquid during fractional crystallisation of an early melt; the sulfides being
638 preserved within early forming silicate phases. In contrast, a second population of sulfides
639 occupies interstitial and intergranular locations within the peridotite. Their composition is
640 somewhat different to the first population; [Os] is frequently at the sub-ppm level, [Re] is
641 higher and more variable than enclosed sulfides and consequently $^{187}\text{Os}/^{188}\text{Os}$ of these
642 sulfides is more radiogenic, i.e. variable and supra-chondritic, even within a population
643 recovered from a single xenolith (Table 5). The textural relationship of these sulfides with
644 silicate phases suggests that this population of sulfides are secondary and most likely derived
645 from a metasomatic event subsequent to melt depletion. While sulfides entirely enclosed
646 within silicate grains tend to evolve under closed system conditions, interstitial sulfides, by
647 virtue of their textural location in the peridotite, experience open system behaviour and are
648 prone to melting, dissolution or physical displacement by any transient melt or fluid. As such,
649 their composition can be modified by mixing of interstitial sulfides of different ages and / or
650 Re/Os ratios, possibly accounting for the wide range of Re/Os ratios in interstitial sulfides.
651 This is notwithstanding the possible additions to the Re and Os budget of interstitial sulfides
652 from Re and / or radiogenic Os fluxed from basaltic material mixed back into the convecting
653 mantle, although the relative quantity of these elements in interstitial sulfides from this source
654 is difficult to quantify. The logical extension of these observations is that bulk-rock Re-Os
655 systematics of peridotite xenoliths will therefore be governed by the relative proportions of
656 these two sulfide populations; the exact nature of an individual xenolith being determined by
657 the abundance of each sulfide population. Figure 6 demonstrates the contribution of these two
658 populations of sulfide in four samples from this study. Mass balance calculations show that in
659 most cases the difference in [Os] between sulfide populations is sufficiently high that,

assuming similar abundances of each population, the contribution from low concentration, interstitial (i.e. metasomatic) sulfide is small and does not markedly affect the whole rock Os isotope ratio. Figure 6 also confirms that the proportion of whole rock Os that can be accounted for by the contributions of olivine, orthopyroxene, clinopyroxene and spinel in 4 samples from this study is <5 % of the whole rock Os budget and in the case of KH03-21 as little as 2.4 %.

While a simple mass balance calculation reveals that KH03-24 does not require a contribution from interstitial sulfides to account for its measured bulk-rock Os abundance and isotope ratio, radiogenic interstitial sulfides with low [Os], high [Re], were sampled from this xenolith (Table 5). Consequently, this suggests that the significantly greater [Os] of enclosed sulfides vastly outweighs the contribution to the Os budget of the interstitial grains. The majority of the sulfide grains analysed from KH03-16 are interstitial (see Table 5). However, to balance the bulk-rock Os isotope ratio of KH03-16 an unradiogenic component is required. Bulk-rock S analyses, which limit the amount of sulfide available for mass balance calculations, suggests that as little as 0.02 wt % of typical enclosed sulfide would balance the whole rock Os isotope ratio and Os concentration of xenolith KH03-16. However the most unradiogenic enclosed sulfides, which must be present, were not recovered from this xenolith. Therefore, the contribution to the bulk rock Os budget from each population of sulfide can only be estimated for KH03-16. In order to balance the whole rock Os isotope ratio the interstitial sulfides cannot contribute more than 17.5 % of the whole rock budget, but with the knowledge of the [Os] of enclosed sulfides from other Kilbourne Hole xenoliths the contribution from interstitial sulfides is probably significantly less. The Os isotope ratio of KH03-15 is too radiogenic to be accounted for by the sum of the contributions from the silicates and spinel plus an overwhelming contribution from enclosed sulfides alone. A relative contribution of 3.5% from interstitial sulfide is sufficient to balance the bulk-rock Os isotope

ratio and bulk-rock [Os]. A similar calculation to that of KH03-15 is required for KH03-21, except a greater contribution (<17.5 %) must come from interstitial sulfides to balance the whole rock Os systematics. When metasomatic, interstitial sulfide is present in these quantities bulk-rock $^{187}\text{Os}/^{188}\text{Os}$ will deviate significantly from the Os isotope signature of a xenolith whose [Os] is dominated by enclosed sulfides.

With the exception of KH03-21, the effects of metasomatic, interstitial sulfide on the Os isotope ratio of the whole rock are of little consequence. Only in samples where the abundance of radiogenic, low [Os], interstitial sulfide is so great as to skew the whole rock Os isotope ratio are whole rock $^{187}\text{Os}/^{188}\text{Os}$ ratios unrepresentative of their enclosed sulfides. Nevertheless, in peridotite xenoliths elsewhere, when the abundance of interstitial metasomatic sulfides is higher, an early melt depletion signature may easily be obscured and bulk-rock Re-Os systematics will only describe a mixture of metasomatic sulfide and earlier melt depletion-related sulfides, thus yielding nothing more than a meaningless “average” Os isotope ratio. For example, bulk-rock T_{RD} can vastly underestimate the timing of melt depletion by up to 0.5 Ga (e.g. Harvey et al., 2006). Figure 7 illustrates the relationship between bulk-rock Re-Os systematics of KH03-15, KH03-16, KH03-21 and KH03-24 and their constituent components. In all cases the bulk-rock $^{187}\text{Os}/^{188}\text{Os}$ appears to be strongly controlled by enclosed sulfides, mainly as a result of their high [Os] (Table 5). In general, the xenoliths appear to have at least one silicate phase that resembles the $^{187}\text{Os}/^{188}\text{Os}$ of the bulk-rock. However the [Os] of these phases (Table 3 and Figure 7) is insufficient to exert a significant control on bulk rock [Os] and therefore bulk-rock $^{187}\text{Os}/^{188}\text{Os}$. Consequently, in peridotite xenoliths in general, bulk-rock T_{RD} ages are often unlikely to reflect an early melt depletion event, especially when a large proportion of the peridotite sulfide budget comes from the interstitial, secondary or metasomatic population. A more accurate appraisal of early melt depletion is more likely derived from the analysis of individual enclosed sulfide grains

that have been protected from subsequent metasomatism. For example, the bulk-rock T_{RD} age of KH03-15 (Table 1) underestimates the age of the oldest sulfide analysed from the same bulk-rock sample by >400 Ma. Similarly, the bulk-rock T_{RD} age of KH03-24 is 150 Ma younger than the oldest enclosed sulfide recovered from that xenolith.

The low sulphur concentrations of the Kilbourne Hole xenoliths of this study suggests that a large proportion of their original sulphur has been lost prior to transport to the surface in the host basalt. Sulphur concentrations for KH03-15, KH03-16, KH03-21 and KH03-24 are all below 50 ppm (KH03-16 [S] <10 ppm), significantly below that expected for fertile mantle ([S] = 200 ± 40 ppm, O'Neil, 1991). Consequently, as sulfide is likely the dominant phase for [S] in peridotite this implies that a significant proportion of sulfide has also been lost, which may, at least in part, account for the low [Os] when compared to the primitive mantle. However, low [S] is not ubiquitous in sub-continental lithospheric mantle xenoliths and therefore this mechanism is unlikely to be universal (e.g. Reisberg et al., 2005). Moreover, the interstitial nature of one of the populations of sulfide suggests that it is more likely to be mobile and prone to alteration under a wide range of circumstances, e.g. supergene weathering (e.g. Lorand et al., 2003), melt depletion and / or metasomatism (e.g. Handler et al., 1999) than those sulfides enclosed within a host silicate grain with no exposure to grain boundary processes.

5.3 Control of HSE abundances by multiple sulfide populations during partial melting

5.3.1 Osmium concentrations and $^{187}\text{Os}/^{188}\text{Os}$ in EM-basalts

The generation of basaltic magma requires partial melting of a peridotite precursor material, the exact melt composition being dependent upon the pressure, temperature, $f\text{O}_2$ and

the composition of the source reservoir. It is, for instance, the variability in the composition of EM-basalts that has often been attributed to the variability in the source material; their heterogeneity being ascribed to various discrete, yet compositionally distinct mantle reservoirs variously refertilised or enriched with recycled basaltic and / or sedimentary material as a result of ongoing subduction and mixing (Zindler & Hart, 1986; Hofmann 1997). The contrasting physical properties of these re-introduced components has been suggested to be responsible for their resistance to complete re-mixing back into the asthenospheric mantle to produce a single homogeneous reservoir from which subsequent basalt can be extracted (e.g. Allègre & Turcotte, 1986; Hart, 1988; Manga, 1996). It has long been accepted that the re-melting of these recycled components generates the distinctive isotopic flavour of the various EM-basalts; their Sr-Nd-Pb isotope composition being geographically restricted and reflecting the mixture of melt derived from asthenospheric mantle and its enriched sub-reservoirs. While this explanation of EM-basalt heterogeneity is robust for isotope systems that are reliant upon lithophile elements (Rb-Sr, Sm-Nd, Pb-Pb, etc) it has recently been suggested that in order to account for the wide range of Re-Os isotope heterogeneity in EM-basalts, and Grande Comore EM-basalts in particular (e.g. Class et al., 2009), additional enriched mantle reservoirs are required.

Despite the apparent incompatibility of Os in silicate minerals, demonstrated both experimentally (Fleet et al., 1991, 1996; Brenan et al., 2003, 2005) and measured in natural samples (Hart & Ravizza, 1996; Burton et al., 1999; Harvey et al., 2010; this study) there is insufficient Os within the silicate phases to produce a significant volume of EM-basalt with the observed range of [Os], even at very low degrees of partial melting – the meagre Os budget in the silicate minerals is quickly exhausted and massively diluted during the melting of the silicate phases. This is in contrast to the lithophile element-based isotope systems whose parent and daughter elements (e.g. Rb, Sr, Sm, Nd, U, Pb) are present in much greater

760 abundances within the silicate minerals that produce the basaltic melt. The Os budget of EM-
 761 basalts is much more likely derived from mantle sulfide which hosts the vast majority of
 762 mantle Os. Mobilisation of this sulfide and its incorporation into a basaltic partial melt is
 763 therefore a far more plausible mechanism for producing a wide range of Os isotope ratios in
 764 EM-basalts and, moreover, the wide range of [Os] observed worldwide. A simple two stage
 765 model demonstrates that the entire range of EM-basalt Os isotope and elemental abundances
 766 can be produced by the sequential incorporation of (i) interstitial sulfide with sub ppm [Os]
 767 and radiogenic $^{187}\text{Os}/^{188}\text{Os}$ followed by (ii) the gradual addition of sulfide grains formerly
 768 enclosed within silicate grains which, as melt depletion intensifies, become exposed to the
 769 melting process as their host grains themselves start to melt. These formerly enclosed
 770 sulfides, randomly oriented within their host grains, then contribute their high [Os] and
 771 comparatively unradiogenic $^{187}\text{Os}/^{188}\text{Os}$ to the basaltic melt. Figure 8 illustrates this process
 772 and demonstrates schematically that with a representative range of mantle sulfides the entire
 773 range of both [Os] and Os isotope ratios can be produced from simple batch melting. As
 774 discussed above, melting of the silicate minerals can only produce a very limited range of
 775 [Os] and will not account for any great variability in $^{187}\text{Os}/^{188}\text{Os}$ given a broadly chondritic
 776 starting material. The range of melt compositions from the silicate components alone is
 777 shown in Figure 10 (white box). This is derived from 1-10 % batch melting of sulfide-free
 778 silicates whose compositions were determined in this study, Burton et al. (1999) and Harvey
 779 et al. (2010). A very limited range of small volume melts can be produced even when
 780 $D_{\text{Os}}^{\text{silicate/melt}}$ is varied by up to an order of magnitude. Interstitial sulfide, with its particularly
 781 low melting temperature compared to that of silicate minerals (Hsieh et al., 1987; Eggler and
 782 Lorand, 1993), will become mobilized and incorporated into the melt very early in the partial
 783 melting process. As soon as melt forms an interconnected network around grain boundaries
 784 then the contribution of interstitial sulfide to the Os budget of the basalt can be added

(process 1 on Figure 8). However, this may only occur at higher temperatures than those at which sulfide would physically melt (e.g. Bockrath et al., 2004; Ballhaus et al. 2006) as sufficient silicate melting will need to occur before sulfide can be mobilised (the mobility of interstitial sulfide in silicate melts during partial melting is summarized in Rudnick & Walker, 2009). With continuing melt depletion enclosed sulfide grains, randomly oriented with regard to their proximity to silicate grain boundaries, will progressively be exposed and thus incorporated into the melt, rapidly increasing the basalt [Os] and lowering the overall $^{187}\text{Os}/^{188}\text{Os}$ (process 2, Figure 10). For example, using the range of [Os] and $^{187}\text{Os}/^{188}\text{Os}$ for Kilbourne Hole interstitial sulfides alone it is possible to produce basalts with a range of Os isotope ratios between approximately that of primitive upper mantle (PUM $^{187}\text{Os}/^{188}\text{Os} = 0.130$; Meisel et al., 2001) and 0.170, and with [Os] of <100 ppt to c. 270 ppt. This is readily achieved by mixing the results of up to 10% batch melting of a typical PUM silicate assemblage and adding less than 0.01 modal % of Kilbourne Hole interstitial sulfide, i.e. an amount of sulfide well within the range of modal abundances measured by e.g. Luguet et al. (2003). Using the range of cratonic sulfides from Griffin et al., (2004), the full range of Os elemental and isotope systematics of Comores EM-basalts, the extreme $^{187}\text{Os}/^{188}\text{Os}$ end-member of EM-basalt, can be generated with an order of magnitude less sulfide. The range of higher [Os] and less radiogenic EM-basalts is then easily accommodated by the gradual addition of formerly enclosed sulfides with high [Os] and generally sub-chondritic $^{187}\text{Os}/^{188}\text{Os}$. Although only two examples are calculated here these two solutions are not numerically unique and various combinations of geologically reasonable sulfide populations with both normal [Os] and $^{187}\text{Os}/^{188}\text{Os}$ allow the Os systematics of the full range of EM-basalts, and most ocean island basalts (OIB) in general to be generated.

5.3.2 The influence of sulfide on EM-basalt PGE systematics

810

811 The early mobilisation of interstitial sulfides followed by the later incorporation of
812 formerly enclosed sulfides is also supported by the observed behaviour of other platinum
813 group elements (PGE). Previous studies of the two discrete populations of mantle sulfides
814 have shown that Os-rich enclosed sulfides are also rich in Ir and Ru (IPGEs) but, compared to
815 interstitial sulfides, are depleted in Pt, Pd (PPGEs) and, as previously discussed, Re (Lorand
816 & Alard, 2001; Aulbach et al., 2004; Bockrath et al., 2004; Mungall & Su, 2005). The early
817 incorporation of PPGEs into MORB has also been demonstrated to be responsible for the
818 apparent PGE and Os-isotopic gap between MORB, ocean island basalts (OIB) and their
819 mantle sources (Alard et al., 2005; Luguet et al., 2008). Consequently, the behaviour of any
820 two IPGE in bulk-rock peridotite during partial melting should be strongly correlated, as
821 should that of any two PPGE as the two populations of sulfide, each with a distinctive
822 composition, contribute to the basaltic melt in a predictable, but different way. Conversely, it
823 would be expected that no significant correlation would be observed between an IPGE and a
824 PPGE in peridotites over an interval of melt depletion. Figure 9a demonstrates an excellent
825 correlation in bulk-rock peridotite abundances of pairs of IPGE, i.e. Ir_N vs. Os_N & (where X_N
826 is $[X]$ normalised to the composition of CI chondrite, after Horan et al., 2003) over the range
827 of melt depletion experienced by the peridotites of this study. Similarly PPGE, e.g. Pd_N vs.
828 Pt_N , demonstrate a similar behaviour ($R^2 > 0.9$, with the exclusion of KH03-16), albeit
829 because of the mobilization of a different sulfide population. However, very little co-variation
830 between individual IPGE vs. individual PPGE exists (Pt_N vs. Os_N). This strongly suggests
831 that the behaviour of IPGE and PPGE during melt depletion is controlled by different phases,
832 i.e. the two compositionally distinct populations of interstitial (high PPGE/IPGE) and
833 enclosed (low PPGE/IPGE) sulfide. This observation is not unique to this particular locality
834 and although the co-variation is not as statistically robust when worldwide peridotites are

835 considered (Figure 9b) the positive co-variation between individual IPGE is still evident in
836 other non-cratonic peridotite xenoliths (Lorand & Alard, 2001; Lorand et al., 2003; Wittig et
837 al, 2010), cratonic peridotite xenoliths (Pearson et al., 2004; Ivanov et al., 2008), orogenic
838 peridotites (e.g. van Acken et al., 2010), abyssal peridotites (e.g. Luguet et al., 2001, 2003,
839 2004) and ophiolitic peridotite (Hanghøj et al., 2010). The notion that IPGE and PPGE
840 mobility, and hence their contribution to basaltic magmas during partial melting of peridotite,
841 is controlled by two separate phases is also supported by the PGE distribution amongst
842 mantle sulfides themselves. Strong correlations between Ir_N vs. Os_N ($R^2 > 0.99$) in sulfides
843 from non-cratonic peridotite (Lorand & Alard, 2001), cratonic peridotite (Aulbach et al.,
844 2004) and abyssal peridotites (Luguet et al., 2001, 2003, 2004) are evident (Figure 9c) and
845 demonstrate that sulfide is the primary control on the behaviour of PGE and Re during melt
846 extraction. Although the co-variation is not as strong between sulfide PPGE, the general trend
847 is still compelling. The net result of the preferential incorporation initially of interstitial
848 sulfide followed by the gradual addition of enclosed sulfide with increasing degrees of partial
849 melting is then clear. The strong correlations between paired IPGE and paired PPGE in
850 peridotitic sulfide (Figure 9c) and lack of correlation between individual IPGE and PPGE
851 illustrates that the two populations of sulfide are the main control on PGE abundance in
852 peridotites not just from this study (Figure 9a) but non-cratonic, cratonic, abyssal and
853 ophiolitic peridotites worldwide (Figure 9b). Moreover, the consistent and predictable
854 behaviour of mantle sulfide during partial melting is evident when the PGE composition of
855 worldwide basalts are examined; the same consistent behaviour of IPGE and PPGE is also
856 evident in basalts irrespective of tectonic setting (Figure 9d) – the PGE abundances and Os
857 isotope composition of basaltic magma can be explained simply by the contribution of first
858 one population of sulfide, with a high PPGE/IPGE, followed by gradual addition of formerly
859 enclosed sulfide with low PPGE/IPGE controls.

Using continental peridotites to derive the composition of oceanic basalts may not always be appropriate as SCLM has invariably been isolated from the convecting mantle for longer and hence likely experienced more metasomatic input than its sub-oceanic counterpart. However, in the case of the peridotites used for this study the choice of material appears justified. In selecting petrographically and texturally simple peridotites that last equilibrated at or near the local asthenosphere / lithosphere boundary the protogranular lherzolites and harzburgites share a number of features with similar oceanic peridotites. Mean Os isotope ratios for abyssal peridotites ($^{187}\text{Os}/^{188}\text{Os} = 0.1236$; Snow & Reisberg, 1995; Brandon et al., 2000; Harvey et al., 2006; Liu et al., 2008) are similar to the Kilbourne Hole peridotites used here ($^{187}\text{Os}/^{188}\text{Os} = 0.1256$) and when the exceptionally depleted abyssal peridotites of Harvey et al. (2006) are excluded are almost indistinguishable from each other (abyssal peridotite $^{187}\text{Os}/^{188}\text{Os} = 0.1257$; Snow & Reisberg, 1995; Brandon et al., 2000; Liu et al., 2008). Abundances of PGE are also similar in oceanic mantle and SCLM, both in terms of absolute abundances and co-variation of paired IPGE and PPGE in bulk-rock peridotite (Fig 9b) and sulfides derived from them (Fig 9c; cf. Luguet et al., 2001, 2003, 2004) so during melt depletion of both these types of peridotite the redistribution of PGE as a result of sulfide mobility should be comparable. However, caution should be exercised in the choice of material used where for example high S abundances could be the result of large quantities of metasomatic sulfide, in texturally complex peridotites, or where bulk-rock PGE abundances materially differ from those of abyssal peridotites.

The possible contribution of PGE from sources other than peridotite-sourced sulfides should also be considered. Many EM-basalts, and OIB in general, are considered to be the product of mixed-source melting with varying proportions being derived from pyroxenite and peridotite (e.g. Hirschmann & Stolper, 1996; Sobolev et al., 2005; 2007). While pyroxenites also contain a significant sulfide fraction it has been demonstrated that in all cases, sulfides

recovered from pyroxenite xenoliths (e.g. Wang et al., 2009; Sen et al., 2010) and non-xenolithic pyroxenites (e.g. van Acken et al., 2010) contain 1-3 orders of magnitude less PGE than their peridotitic counterparts. Thus it would seem unlikely that even in instances where the production of basaltic melt is dominated by the melting of pyroxenite, the contribution to the basalt PGE budget, and hence Os isotope systematics, will be quickly overprinted by the contribution from peridotite hosted sulfide. A model that accounts for the combined contributions of sulfide from mixed source melting has been proposed by Luguet et al. (2008). Their model suggests that during the melting of a pyroxenite – peridotite source the early melting of pyroxenite results in reaction with the peridotite wall-rock (e.g. Yaxley and Green 1998) creating a source rock containing sulfides from both peridotite and pyroxenite. This reacted wallrock then provides the source for low solidus metasomatic sulfides which are readily incorporated into the basaltic melt; the overall PGE signature being dominated by the contribution from the peridotite source rock. Luguet et al. (2008) also go on to speculate about the possible contribution to basalt PGE and $^{187}\text{Os}/^{188}\text{Os}$ systematics from refractory alloy phases. However it seems difficult to reconcile the physical and chemical properties of these phases (i.e. refractory, dense, unreactive) with the incorporation and / or redistribution into a basaltic melt. In summary, based upon the relative PGE budgets of peridotite and pyroxenite, combined with the unfavourable physical and chemical properties of PGE-rich alloys, the Os isotope systematics of EM-basalts in particular and OIB in general are most likely controlled by peridotite-hosted sulfides.

6. CONCLUDING REMARKS

Bulk-rock PGE, Re-Os elemental and isotope systematics of peridotites, and consequently OIB, including EM-basalts, are controlled by volumetrically insignificant sulfides. More than one population of sulfides, which have large compositional differences between the populations in terms of major elements, PGE and Re-Os elemental and isotope systematics, are commonly present in peridotite samples. This means that bulk-rock Re-Os isotope systematics of peridotite are often merely the aggregate signatures of two populations of sulfide, produced at different times and under different conditions, thus rendering bulk-rock Re-Os isotope geochronology extremely difficult to interpret in all but the most straightforward of examples.

The textural characteristics of the two populations of sulfide govern their behaviour during partial melting; interstitial, metasomatic sulfides being liberated from their peridotite host during the early stages of partial melting, whereas sulfides enclosed within silicate grains only becoming exposed to the generated melt as their host grains themselves start to contribute to the production of basalt. The wide range of mantle sulfide compositions present even within a single peridotite xenolith or within a small number of xenoliths from a restricted geographical area can easily account for the Os compositional and isotopic range of EM-basalts. There is therefore no need for additional mantle reservoirs to account for the apparent co-variation of lithophile-element based and siderophile-element based isotope systems in the generation of EM-basalts.

ACKNOWLEDGEMENTS

We would like to thank John Watson for assistance with the XRF measurements and Andy Tindle for his help with the electron microprobe at The Open University. Funding for this research was provided by NERC grant NER/A/S/2001/00538 which has allowed J.H. to undertake the isotope measurements presented here.

REFERENCES

- Ackerman, L., Walker, R.J., Puchtel, I.S., Pitcher, L., Jelnek, E., Strnad, L. (2009) Effects of melt percolation on highly siderophile elements and Os isotopes in subcontinental lithospheric mantle: A study of the upper mantle profile beneath Central Europe. *Geochim. Cosmochim. Acta* **73**, 2400-2414.
- Alard, O., Griffin, W.L., Pearson, N.J., Lorand, J.-P., O'Reilly, S.Y. (2002) New insights into the Re-Os systematics of sub-continental lithospheric mantle from in-situ analysis of sulphides. *Earth Planet. Sci. Lett.* **203**, 651-663.
- Alard, O., Luguet, A., Pearson, N.J., Griffin, W.L., Lorand, J.-P., Gannoun, A., Burton, K.W., O'Reilly, S.Y. (2005) In-situ Os isotopes in abyssal peridotites bridge the isotopic gap between MORBs and their source mantle. *Nature* **436**, 1005-1008.
- Allègre, C.J., Turcotte, D.L. (1986) Implications of a two-component marble cake mantle. *Nature* **323**, 123-127.
- Aulbach, S., Griffin, W.F., Pearson, N.J., O'Reilly, S.Y., Kivi, K., Doyle, B.J. (2004) Mantle formation and evolution, Slave Craton: constraints from HSE abundances and Re-Os isotope systematics of sulphide inclusions in mantle xenocrysts. *Chem. Geol.* **208**, 61-88.
- Ballhaus, C., Sylvester, P. (1999) Noble metals enrichment processes in the Merensky Reef, Bushveld Complex. *J. Petrol.* **41**, 546-561.

982 Ballhaus, C., Bockrath, C., Wohlgemuth-Ueberwasser, C., Laurenz, V., Berndt, J., (2006)
 983 Fractionation of the noble metals by physical processes. *Contrib. Mineral. Petrol.* **152**,
 984 667–684.
 985
 986 Basaltic Volcanism Study Project (1981). *Basalt volcanism on the terrestrial planets*.
 987 Pergamon Press Inc, New York, 1286 pp.
 988
 989 Becker, H., Horan, M.F., Walker, R.J., Gao, S., Lorand, J.-P., Rudnick, R.L. (2006) Highly
 990 siderophile element composition of the Earth's primitive upper mantle: Constraints from
 991 new data on peridotite massifs and xenoliths. *Geochim. Cosmochim. Acta* **70**, 4528-4550.
 992
 993 Bennett, V.C., East, T.M., Norman, M.D. (1996) Two mantle plume components in Hawaiian
 994 picrites inferred from correlated Os-Pb isotopes. *Nature* **381**, 67-83.
 995
 996 Birck, J.-L., Roy-Barman, M., Capmas F. (1997) Re–Os isotopic measurements at the
 997 femtomole level in natural samples. *Geostand. Newslett.* **20**(1), 19–27.
 998
 999 Bockrath, C., Ballhaus, C., Holzheid, A. (2004) A mechanism for the fractionation of highly
 1000 siderophile elements during mantle melting. *Science* **305**, 1951-1953.
 1001
 1002 Brandon, A.D., Becker, H., Carlson, R.W., Shirey, S.B. (1999) Isotopic constraints on
 1003 timescales and mechanisms of slab material transport in the mantle wedge: evidence for
 1004 the regional uniformity of CO₂ and H₂O rich fluids in lithospheric mantle. *Earth Planet.*
 1005 *Sci. Lett.* **160**, 387-407.
 1006

1007 Brandon, A.D., Snow, J.E., Walker, R.J., Morgan, J.W., Mock, T.D. (2000). ^{190}Pt – ^{186}Os and
 1008 ^{187}Re – ^{187}Os systematics of abyssal peridotites. *Earth Planet. Sci. Lett.* **177**, 319-355.
 1009
 1010 Brandon, A.D., Graham, D.W., Waight, T., Gautason, B. (2007) ^{186}Os and ^{187}Os enrichments
 1011 and high $^3\text{He}/^4\text{He}$ sources in the Earth's mantle: evidence from Icelandic picrites.
 1012 *Geochim. Cosmochim. Acta* **71**, 4570-4591.
 1013
 1014 Brenan, J.M., McDonough, W.F., Dalpé, C. (2003) Experimental constraints on the
 1015 partitioning of rhenium and some platinum-group elements between olivine and silicate
 1016 melt. *Earth Planet. Sci. Lett.* **212**, 135-150.
 1017
 1018 Brenan, J.M., McDonough, W.F., Ash, R. (2005) An experimental study of the solubility and
 1019 partitioning of iridium, osmium and gold between olivine and silicate melt. *Earth Planet.*
 1020 *Sci. Lett.* **237**, 855-872.
 1021
 1022 Burnham, O.M., Rogers, N.W., Pearson, D.G., van Calsteren, P., Hawkesworth, C.J. (1998)
 1023 The petrogenesis of the eastern Pyrrhenian peridotites: An integrated study of their whole-
 1024 rock geochemistry and Re-Os isotope composition. *Geochim. Cosmochim. Acta* **62**, 2293-
 1025 2310.
 1026
 1027 Burton, K.W., Schiano, P., Birck, J.-L., Allègre, C.J. (1999) Osmium isotope disequilibrium
 1028 between mantle minerals in a spinel-lherzolite. *Earth Planet. Sci. Lett.* **172**, 311-322.
 1029

1030 Burton, K.W., Gannoun, A., Birck, J-L., Allegre, C.J., Schiano, P., Clocchiatti, R., Alard, O.
 1031 (2002) The compatibility of rhenium and osmium in natural olivine and their behaviour
 1032 during melting and basalt genesis. *Earth Planet. Sci. Lett.* **198**, 63-76.
 1033
 1034 Bussod, G.Y.A. (1981) Thermal and kinematic history of mantle xenoliths from Kilbourne
 1035 Hole, New Mexico. (*MSc thesis*). University of Washington, Seattle. 72pp.
 1036
 1037 Bussod, G.Y.A., Irving, A.J. (1981) Thermal and rheological history of the upper mantle
 1038 beneath the southern Rio Grande Rift: evidence from Kilbourne Hole xenoliths. In: *Papers*
 1039 *presented to the conference on the proceedings of planetary rifting*. Lunar and Planetary
 1040 Institute. Contribution No. **457**, 145-148.
 1041
 1042 Bussod, G.Y.A., Williams, D.R. (1991) Thermal and kinematic model of the southern Rio
 1043 Grande rift: inferences from crustal and mantle xenoliths from Kilbourne Hole, New
 1044 Mexico. *Tectonophysics* **197**, 373-389.
 1045
 1046 Cabri, L. (1992) The distribution of trace metals in minerals and mineral products, *Mineral.*
 1047 *Mag.* **56**, 289-308.
 1048
 1049 Carlson R.W., Irving A.J. (1994) Depletion and enrichment history of sub-continental
 1050 lithospheric mantle: an Os, Sr, Nd and Pb isotopic study of ultramafic xenoliths from the
 1051 northwestern Wyoming craton. *Earth Planet. Sci. Lett.* **126**, 457-472.
 1052
 1053 Carter, J.L. (1965). The origin of olivine bombs and related inclusions in basalts (*PhD*
 1054 *thesis*). Rice University, Houston. 275pp.

1055

1056 Chu, Z.-Y., Wu, F.-Y., Walker, R.J., Rudnick, R.L., Pitcher, L., Puchtel, I.S., Yang, Y.-H.,
 1057 Wilde, S.A. (2009) Temporal evolution of the lithospheric mantle beneath the East North
 1058 China craton. *J. Petrol.* **50**, 1857-1898.

1059

1060 Class, C., Goldstein, S.L., Shirey, S.B. (2009) Osmium isotopes in Grande Comore lavas: a
 1061 new extreme among a spectrum of EM-type mantle endmembers. *Earth Planet. Sci. Lett.*
 1062 **284**, 219-227.

1063

1064 Cohen, A.S., Waters, F.G. (1996) Separation of osmium from geological materials by solvent
 1065 extraction for analysis by TIMS. *Anal. Chim. Acta* **332** 269–275.

1066

1067 Coisy P., Nicolas A. (1978) Regional structure and geodynamics of the upper mantle beneath
 1068 the Massif Central. *Nature* **274**, 429–432.

1069

1070 Creaser, R.A., Papanastassiou, D.A., Wasserburg, G.J. (1991) Negative thermal ion mass
 1071 spectrometry of osmium, rhenium, and iridium. *Geochim. Cosmochim. Acta* **55**, 397–401.

1072

1073 Dale, C.W., Luguet, A., Macpherson, C.G., Pearson, D.G., Hickey-Vargas, R. (2008)
 1074 Extreme platinum-group element fractionation and variable Os isotope compositions in
 1075 Philippine Sea Plate basalts: tracing mantle source heterogeneity. *Chem. Geol.* **248**, 213–
 1076 238.

1077

1078 Day, J.M.D., Pearson, D.G., MacPherson, C.G., Lowry, D., Carracedo, J.C. (2009)
 1079 Pyroxenite-rich mantle formed by recycled oceanic lithosphere: oxygen-osmium isotopic
 1080 evidence from Canary Island lavas. *Geology* **37**, 555-558.
 1081
 1082 Debaille, V., Troennes, R.G., Brandon, A.D., Waight, T.E., Graham, D.W., Lee, C.-T.A
 1083 (2009) Primitive off rift basalts from Iceland and Jan Mayen: osmium isotopic evidence
 1084 for a mantle source containing enriched sub-continental lithosphere. *Geochim.*
 1085 *Cosmochim. Acta* **73**, 3423-3449.
 1086
 1087 Dromgoole, E.L., Pasteris, J.D. (1987) Interpretation of the sulphide assemblages in a suite of
 1088 xenoliths from Kilbourne Hole, New Mexico. *Geol. Soc. Am. Spec. Pap.* **215**, 25–46.
 1089
 1090 Eggler D. H., Lorand J.-P. (1993) Mantle sulfide oxybarometry. *Geochim. Cosmochim. Acta*
 1091 **57**, 2213–2222.
 1092
 1093 Eisele, J., Sharma, M., Galer, S.J.G., Blichert-Toft, J., Devey, C.W., Hofmann, A.W. (2002)
 1094 The role of sediment recycling in EM-1 inferred from Os, Pb, Hf, Nd, Sr isotope and trace
 1095 element systematics of the Pitcairn hotspot. *Earth Planet. Sci. Lett.* **196**, 197-212.
 1096
 1097 Escrig, S., Schiano, P., Schilling, J.-G., Allègre, C.J. (2005) Rhenium-osmium isotope
 1098 systematics in MORB from the Southern Mid-Atlantic Ridge (40°-50°S). *Earth Planet.*
 1099 *Sci. Lett.* **235**, 528-548.
 1100

1101 Fleet, M.E., Stone, W.E., Crocket, J.H. (1991) Partitioning of palladium, iridium, and
 1102 platinum between sulphide liquid and basalt melt: Effects of melt composition,
 1103 concentration and oxygen fugacity. *Geochim. Cosmochim. Acta* **55**, 2545-2554.
 1104

1105 Fleet, M.E., Crocket, J.H., Stone, W.E. (1996) Partitioning of platinum group elements (Os,
 1106 Ir, Ru, Pt, Pd) and gold between sulphide liquid and basalt melt. *Geochim. Cosmochim.*
 1107 *Acta* **60**, 2397-2412.
 1108

1109 Frey F.A., Green, D.H. (1974) The mineralogy, geochemistry and origin of lherzolite
 1110 inclusions in Victorian basanites. *Geochim. Cosmochim. Acta* **38**, 1023–1059.
 1111

1112 Gaffney, A.M., Nelson, B.K., Reisberg, L., Eiler, J.M. (2005) Oxygen-osmium isotope
 1113 systematics of West Maui lavas: a record of shallow-level magmatic processes. *Earth*
 1114 *Planet. Sci. Lett.* **239**, 122-139.
 1115

1116 Galer, S.J.G., O’Nions, R.K. (1989) Chemical and isotopic studies of ultramafic inclusions
 1117 from the San Carlos Volcanic Field, Arizona: a bearing on their petrogenesis. *J. Petrol.* **30**,
 1118 1033–1064.
 1119

1120 Gannoun, A., Burton, K.W., Thomas, L.E., Parkinson, I.J., van Calsteren, P.W., Schiano, P.
 1121 (2004) Osmium isotope heterogeneity in the constituent phases of mid-ocean ridge basalts.
 1122 *Science* **303**, 70-72.
 1123

1124 Gannoun, A., Burton, K.W., Parkinson, I.J., Alard, O., Schiano, P., Thomas, L.E. (2007) The
 1125 scale and origin of the osmium isotope variations in mid-ocean ridge basalts. *Earth Planet.*
 1126 *Sci. Lett.* **259**, 541-556.
 1127
 1128 Griffin, W.L., O'Reilly, S.Y., Abe, N., Aulbach, S., Davies, R.M., Pearson, N.J., Doyle, B.J.,
 1129 Kivi, K. (2003) The origin and evolution of Archean lithospheric mantle. *J. PreCam. Res.*
 1130 **127**, 19-41.
 1131
 1132 Griffin, W.L., Graham, S., O'Reilly, S.Y., Pearson, N.J. (2004) Lithosphere evolution
 1133 beneath the Kaapvaal craton: Re-Os systematics of sulphides in mantle derived peridotites.
 1134 *Chem. Geol.* **208**, 89-118.
 1135
 1136 Hammond, S.J., Yoshikawa, M., Harvey, J., Burton, K.W. (2010). Multiple metasomatic
 1137 events recorded in Kilbourne Hole peridotite xenoliths: the relative contribution of host
 1138 basalt interaction vs. silicate metasomatic glass. *AGU Fall 2010 meeting*, abstract **V23b**,
 1139 2413.
 1140
 1141 Handler, M.R., Bennett, V.C. (1999) Behaviour of platinum-group elements in the sub-
 1142 continental mantle of eastern Australia during variable metasomatism and melt depletion.
 1143 *Geochim. Cosmochim. Acta* **63**, 3597-3618.
 1144
 1145 Hanghøj, K., Kelemen, P.B., Hassler, D., Godard, M. (2010) Composition and genesis of
 1146 depleted mantle peridotites from the Wadi-Tayan Massif, Oman ophiolite: major and trace
 1147 element geochemistry, and Os isotope and PGE systematics. *J. Petrol.* **51**, 201-227.
 1148

1149 Hart, S.R. (1988) Heterogeneous mantle domains: signatures, genesis and mixing
 1150 chronologies. *Earth Planet. Sci. Lett.* **90**, 273-296.

1151

1152 Hart, S.R., Ravizza, G. (1996) Os partitioning between phases in lherzolite and basalt. *In*
 1153 *Earth Processes: Reading the Isotopic Code* (eds. Basu, A. and Hart, S. R.) AGU,
 1154 Washington, *Geophys. Mon.* **95**, 123–134.

1155

1156 Harvey, J., Gannoun, A., Burton, K.W., Rogers, N.W., Alard, O., Parkinson, I.J. (2006)
 1157 Ancient melt extraction from the oceanic upper mantle revealed by Re-Os isotopes from
 1158 the Mid-Atlantic Ridge. *Earth Planet. Sci. Lett.* **244**, 606-621.

1159

1160 Harvey, J., Gannoun, A., Burton, K.W., Rogers, N.W., Schiano, P., Alard, O. (2010)
 1161 Unravelling the effects of melt depletion and secondary infiltration on mantle Re–Os
 1162 isotopes beneath the French Massif Central. *Geochim. Cosmochim. Acta* **74**, 293-320.

1163

1164 Hauri, E.H., Lassiter, J.C., DePaulo, D.J. (1996) Osmium isotope systematics of drilled lavas
 1165 from Mauna Loa, Hawaii. *J. Geophys. Res.* **B101**, 11793-11806.

1166

1167 Hauri, E.H., Kurz, M.D. (1997) Melt migration and mantle chromatography 2: A time-series
 1168 Os-isotope study of Mauna Loa volcano, Hawaii. *Earth Planet. Sci. Lett.* **153**, 21-36.

1169

1170 Hauri E.H., Hart S.R. (1997) Rhenium abundances and systematics in oceanic basalts. *Chem.*
 1171 *Geol.* **139**, 185–205.

1172

1173 Hirschmann, M.M., Stolper, E.M. (1996) A possible role for garnet pyroxenite in the origin
 1174 of “garnet signature” in MORB. *Contrib. Mineral. Petrol.* **124**, 185-208.
 1175

1176 Hoffer, J.M. (1976) The Potrillo basalt field, south-central New Mexico. In: Cenozoic
 1177 volcanism in southwestern New Mexico. (Eds) Elston, W., Northrop, S.A. *New Mexico*
 1178 *Geol. Soc. Special Pub.* **5**, 89-92.
 1179

1180 Hofmann, A.W. (1997) Mantle geochemistry: the message from oceanic volcanism. *Nature*,
 1181 **385**, 219-229.
 1182

1183 Holzheid, A. (2010) Separation of sulfide melt droplets in sulphur saturated silicate liquids.
 1184 *Chem. Geol.* **274**, 127-135.
 1185

1186 Horan, M.F., Walker, R.J., Morgan, J.W., Grossman, J.N., Rubin, A.E. (2003) Highly
 1187 siderophile elements in chondrites. *Chem. Geol.* **196**, 27-42.
 1188

1189 Hsieh, J.-C., Vlach, K.C., Chang, Y.A. (1987) The Fe–Ni–S system: I. A thermodynamic
 1190 analysis of the phase equilibria calculation of the phase diagram from 1173 to 1623 K.
 1191 *High Temp. Sci.* **23**, 17–38.
 1192

1193 Ionov, D.A., Dupuy, C., O'Reilly, S.Y., Kopylova, M.G., Genshaft Y.S. (1993) Carbonated
 1194 peridotite xenoliths from Spitzbergen: implications for the trace element signature of
 1195 mantle carbonate metasomatism. *Earth Planet. Sci. Lett.* **119**, 283–297.
 1196

1197 Ireland, T.J., Walker, R.J., Garcia, M.O. (2009) Highly siderophile element and ¹⁸⁷Os isotope
1198 systematics of Hawaiian picrites: implications for parental melt composition and source
1199 heterogeneity. *Chem. Geol.* **260**, 112-128.

1200

1201 Irving, A.J. (1979) Kilbourne Hole spinel lherzolites: samples of multiply depleted, enriched
1202 and deformed mantle. *Abstr. EOS transactions, American Geophysical Union* **60**, 418.

1203

1204 Irving, A.J. (1980) Petrology and geochemistry of composite ultramafic xenoliths in alkali
1205 basalts and implications for magmatic processes in the mantle. *Am. J. Sci.* **280-A**, 389–
1206 426.

1207

1208 Ivanov, A.V., Paleskii, S.V., Demonterova, E.I., Nikolaeva, I.V., Ashchepkov, I.V.,
1209 Rasskazov, S.V. (2008) Platinum-group elements and rhenium in mantle xenoliths from
1210 the East Sayan volcanic field (Siberia, Russia): evaluation of melt extraction and
1211 refertilization processes in lithospheric mantle of the Tuva-Mongolian Massif. *Terra*
1212 *Nova* **20**, 504-511.

1213

1214 Jagoutz, E., Palme, H., Blum, H., Cendales, M., Dreibus, G., Spettel, B., Lorenz, V., Wänke,
1215 H. (1979) The abundances of major, minor and trace elements in the Earth's mantle as
1216 derived from primitive ultramafic nodules. Proceedings of 10th LPSC. *Geochim.*
1217 *Cosmochim. Acta Supplement* **10**, 2031–2051.

1218

1219 Jamais, M., Lassiter, J.C., Brüggmann, G.E. (2008) PGE and Os-isotopic variations in lavas
1220 from Kohala volcano, Hawaii: constraints on PGE behaviour and melt/crust interaction.
1221 *Chem. Geol.* **250**, 16-28.

1222

1223 Kil, Y., Wendlandt, R.F. (2004) Pressure and temperature evolution of upper mantle under
 1224 the Rio Grande rift. *Contrib. Miner. Petrol.* **148**, 2665-2680.

1225

1226 Kuno H., Aoki, K. (1970) Chemistry of ultramafic nodules and their bearing on the origin of
 1227 basaltic magmas. *Phys. Earth Planet. Interiors* **3**, 273–301.

1228

1229 Lassiter, J.C., Hauri, E.H. (1998) Osmium isotope variations in Hawaiian lavas: evidence for
 1230 recycled oceanic lithosphere in the Hawaiian plume. *Earth Planet. Sci. Lett.* **164**, 483-496.

1231

1232 Lassiter, J.C., Hauri, E. H., Reiners, P.W., Garcia, M.O. (2000) Generation of Hawaiian post-
 1233 erosional lavas by melting of a mixed lherzolite/pyroxenite source. *Earth Planet. Sci. Lett.*
 1234 **178**, 269-284.

1235

1236 Lassiter, J.C. (2003) Rhenium volatility in sub-aerial lavas: constraints from sub-aerial and
 1237 submarine portions of the HSDP-2 Mauna Kea drillcore. *Earth Planet. Sci. Lett.* **214**, 311-
 1238 325.

1239

1240 Liu, C.-Z., Snow, J.E., Hellebrand, E., Brügmann, G., von der Handt, A., Büchl, A.,
 1241 Hofmann, A.W. (2008) Ancient, highly heterogeneous mantle beneath Gakkel Ridge,
 1242 Arctic Ocean. *Nature* **452**, 311-316.

1243

1244 Lorand, J.-P., Alard, O. (2001) Platinum-group element abundances in the upper mantle: New
 1245 constraints from in-situ and whole-rock analyses of Massif Central xenoliths (France).
 1246 *Geochim. Cosmochim. Acta* **65**, 2789-2806.

1247

1248 Lorand, J.-P., Alard, O., Luguet, A., Keays, R.R. (2003) Sulphur and selenium systematics of
 1249 the sub-continental lithospheric mantle: Inferences from the Massif Central xenolith suite
 1250 (France). *Geochim. Cosmochim. Acta* **67**, 4137-4151.

1251

1252 Luck J.M., Allègre, C.J. (1983) ^{187}Re - ^{187}Os systematics in meteorites and cosmochemical
 1253 consequences. *Nature* **302**, 130–32.

1254

1255 Luguet, A., Alard, O., Lorand, J.-P., Pearson, N.J., Ryan, C., O'Reilly, S.Y. (2001) Laser
 1256 ablation microprobe (LAM)-ICPMS reveals the highly siderophile element geochemistry
 1257 of the oceanic mantle. *Earth Planet. Sci. Lett.* **189**, 285-294.

1258

1259 Luguet, A., Lorand, J.-P., Seyler, M. (2003) Sulphide petrology and highly siderophile
 1260 element geochemistry of abyssal peridotites: a coupled study of from the Kane Fracture
 1261 Zone (45°W, 23°20'N, MARK Area, Atlantic Ocean). *Geochim. Cosmochim. Acta* **67**,
 1262 1553-1570.

1263

1264 Luguet, A., Lorand, J.-P., Alard, O., Cottin, J.-Y. (2004) A multi-technique study of platinum
 1265 group element systematic in some Ligurian ophiolitic peridotites, Italy. *Chem. Geol.* **208**,
 1266 175-194.

1267

1268 Luguet, A., Pearson, D.G., Nowell, G.M., Dreher, S.T., Coggan, J.A., Spetsius, Z.V., Parman,
 1269 S.W. (2008) Enriched Pt-Re-Os isotope systematics in plume lavas explained by
 1270 metasomatic sulphides. *Science* **319**, 453-456.

1271

1272 Mackovicky, M., Mackovicky, E., Rose-Hansen, J. (1986) Experimental studies on the
 1273 solubility and distribution of platinum group elements in base-metal sulfides in platinum
 1274 deposits, in: *Metallogeny of Basic and Ultrabasic Rocks*. Eds: Gallagher, M.J., Ixer, R.A.,
 1275 Neary, C.R., Prichard, H.M., *Inst. Mineral. Metall.*, pp. 415-425.

1276

1277 Mallmann G., O'Neill H.St.C. (2007) The effect of oxygen fugacity on the partitioning of
 1278 rhenium between crystals and silicate melt during mantle melting. *Geochimica et*
 1279 *Cosmochimica Acta* **71**, 2837-2857.

1280

1281 Manga, M. (1996) Mixing of heterogeneities in the mantle: effect of viscosity differences.
 1282 *Geophys. Res. Lett.* **23** 403–406.

1283

1284 Martin, C.E., Carlson, R.W., Frey, F.A., Chen, C.-Y. (1994) Os-isotopic variation in basalts
 1285 from Haleakala volcano, Maui, Hawaii: a record of magmatic processes in oceanic mantle
 1286 and crust. *Earth Planet. Sci. Lett.* **128**, 287-301.

1287

1288 Marchesi, C., Griffin, W.F., Garrido, C.J., Bodinier, J.-L., O'Reilly, S.Y., Pearson, N.J.
 1289 (2009) Persistence of mantle lithospheric Re-Os isotopic signature during
 1290 asthenospherization of the sub-continental lithospheric mantle: insights from in-situ
 1291 isotopic analyses of sulphides from the Ronda peridotite (Southern Spain). *Contrib.*
 1292 *Mineral. Petrol.* **159**, 315-330.

1293

1294 Meisel, T., Walker, R.J., Morgan, J.W. (1996) The osmium isotopic composition of the
 1295 Earth's upper mantle. *Nature* **383**, 517-520.

1296

1297 Meisel, T., Walker, R.J., Irving, A.J., Lorand, J.P. (2001) Osmium isotopic composition of
 1298 mantle xenoliths: a global perspective. *Geochim. Cosmochim. Acta* **65**, 1311-1323.
 1299

1300 Meisel, T., Reisberg, L., Moser, J., Carignan, J., Melcher, F., Brüggmann, G.E. (2003) Re–Os
 1301 systematics of UB–N, a serpentinised peridotite reference material. *Chem. Geol.* **201**, 161–
 1302 179.
 1303

1304 Meisel, T., Moser, J., Kettisch, P. (2008) Determination of osmium and other platinum group
 1305 elements in chromitites by acid digestion and ICPMS. Department of General and
 1306 Analytical Chemistry, University of Leoben, Leoben, p. 1.
 1307

1308 Morgan, J.W. (1986) Ultramafic xenoliths: clues to Earth's late accretionary history. *J.*
 1309 *Geophys. Res.* **91**, 12375-12387.
 1310

1311 Mungall, J.E., Su, S. (2005) Interfacial tension between magmatic sulphide and silicate
 1312 liquids: constraints on kinetics of sulphide liquation and sulphide migration through
 1313 silicate rocks. *Earth Planet. Sci. Lett.* **274**, 127-135.
 1314

1315 O'Neil, H. St. C. (1991) The origin of the moon and the early history of the Earth – a
 1316 chemical model: Part 2 The Earth. *Geochim. Cosmochim. Acta* **55**, 1159-1172.
 1317

1318 Pearson, D.G., Shirey, S.B., Carlson, R.W., Boyd, F.R., Pokhilenko, N.P., Shimizu, N.
 1319 (1995) Re–Os, Sm–Nd and Rb–Sr isotope evidence for thick Archean lithospheric mantle
 1320 beneath the Siberian craton modified by multistage metasomatism. *Geochim. Cosmochim.*
 1321 *Acta* **59**, 959-977.

1322

1323 Pearson, D.G., Shirey, S.B., Harris, J.W., Carlson, R.W. (1998) Sulphide inclusions in
 1324 diamonds from the Koffiefontein kimberlite, South Africa: constraints on diamond ages
 1325 and mantle Re-Os systematics. *Earth Planet. Sci. Lett.* **160**, 311-326.

1326

1327 Pearson, D.G. (1999) The age of continental roots. *Lithos* **48**, 171-194.

1328

1329 Pearson, D.G., Woodland, S.J. (2000) Carius tube digestion and solvent extraction/ion
 1330 exchange separation for the analysis of PGEs (Os, Ir, Pt, Pd, Ru) and Re–Os isotopes in
 1331 geological samples by isotope dilution ICP-mass spectrometry. *Chem. Geol.* **165**, 87–107.

1332

1333 Pearson, D.G., Irvine, G.J., Ionov, D.A., Boyd, F.R., Dreibus, G.E. (2004) Re–Os isotope
 1334 systematics and platinum group element fractionation during mantle melt extraction: a
 1335 study of massif and xenolith peridotite suites. *Chem. Geol.* **208**, 29–59.

1336

1337 Pearson, N.J., Alard, O., Griffin, W.L., Jackson, S.E., O'Reilly, S.Y. (2002) In situ
 1338 measurement of Re-Os isotopes in mantle sulfides by laser-ablation multi-collector
 1339 inductively coupled plasma mass spectrometry: Analytical methods and preliminary
 1340 results. *Geochim. Cosmochim. Acta* **66**, 1037-1050.

1341

1342 Pegram B.J., Allègre, C.J. (1992) Osmium isotopic compositions from oceanic basalts. *Earth*
 1343 *Planet. Sci. Lett.* **111**, 59–68.

1344

1345 Pitcher, L., Heltz, R.T., Walker, R.W., Piccoli, P. (2009) Fractionation of the platinum-group
 1346 elements and Re during crystallization of basalts in Kilauea Iki Lava Lake, Hawaii. *Chem.*
 1347 *Geol.* **260**, 196–210.
 1348
 1349 Qi, L., Zhou, M.-F. (2008) Platinum-group element and Sr-Nd-Os isotope geochemistry of
 1350 Permian Emeishan flood basalts, in Guizhou Province, SW China. *Chem. Geol.* **248**, 83-
 1351 103.
 1352
 1353 Reid, J.B., Woods, G.A. (1978) Oceanic mantle beneath the southern Rio Grande Rift. *Earth*
 1354 *Planet. Sci. Lett.* **41**, 303-316.
 1355
 1356 Reisberg, L., Zindler, A., Marcantonio, F., White, W., Wyman, D., Weaver, B. (1993) Os
 1357 isotope systematics in ocean island basalts. *Earth Planet. Sci. Lett.* **120**, 149-167.
 1358
 1359 Reisberg, L., Lorand, J.-P. (1995) Longevity of sub-continental mantle lithosphere from
 1360 osmium isotope systematics in orogenic peridotite massifs. *Nature*, **376**, 159-162.
 1361
 1362 Reisberg, L., Zhi, X., Lorand, J.-P., Wagner, C., Peng, Z., Zimmermann, C. (2005) Re-Os
 1363 and S systematics of spinel peridotite xenoliths from east central China: Evidence for
 1364 contrasting effects of melt percolation. *Earth Planet. Sci. Lett.* **239**, 286-308.
 1365
 1366 Richter, K., Chesley, J.T., Geist, D., Ruiz, J. (1998) Behaviour of Re during magma
 1367 fractionation: an example from Volcan Alcedo, Galapagos. *J. Petrol.* **39**, 785-795.
 1368

1369 Righter K., Campbell A.J., Humayun M., Hervig R.L. (2004) Partitioning of Ru, Rh, Pd, Re,
 1370 Ir, and Au between Cr-bearing spinel, olivine, pyroxene and silicate melts. *Geochim.*
 1371 *Cosmochim. Acta* **68**, 867–880.
 1372
 1373 Roden, M.F., Irving, A.J., Murthy, V.R. (1988) Isotopic and trace element composition of
 1374 the upper mantle beneath a young continental rift: Results from Kilbourne Hole, New
 1375 Mexico. *Geochim. Cosmochim. Acta* **52**, 461-476.
 1376
 1377 Ross, C.S., Foster, D.M., Myers, A.T. (1954) Origin of dunites and olivine rich inclusions in
 1378 basaltic rocks. *Am. Mineral.* **39**, 693–737.
 1379
 1380 Roy-Barman, M, Allègre C.J. (1995) $^{187}\text{Os}/^{186}\text{Os}$ in oceanic island basalts: tracing oceanic
 1381 crust recycling in the mantle. *Earth Planet. Sci. Lett.* **129**, 145-161.
 1382
 1383 Rudnick, R.L., Walker, R.J. (2009) Interpreting ages from Re–Os isotopes in peridotites.
 1384 *Lithos* **112S**, 1083-1095.
 1385
 1386 Sen, I.S., Bizimis, M., Sen, G. (2010) Geochemistry of sulphides in Hawaiian garnet
 1387 pyroxenite xenoliths: Implications for highly siderophile elements in the oceanic mantle.
 1388 *Chem. Geol.* **273**, 180-192.
 1389
 1390 Shirey, S.B., Walker, R.J. (1995) Carius tube digestion for low blank rhenium–osmium
 1391 analysis. *Anal. Chem.* **34**, 2134–2141.
 1392

- 1393 Shirey, S.B., Walker, R.J. (1998) The Re-Os isotope system in cosmochemistry and high
1394 temperature geochemistry. *Annu. Rev. Earth Planet. Sci.* **26**, 423-500.
1395
- 1396 Skovgaard, A.C., Storey, M., Baker, J.A., Blusztajn, J. (2001) Osmium-oxygen isotopic
1397 evidence for a recycled and strongly depleted component in the Iceland mantle plume.
1398 *Earth Planet. Sci. Lett.* **194**, 259-275.
1399
- 1400 Snow, J.E., Reisberg, L. (1995). Os isotopic systematics of the MORB mantle: results from
1401 altered abyssal peridotites. *Earth Planet. Sci. Lett.* **133**, 411-421.
1402
- 1403 Sobolev, A.V., Hofmann, A.W., Sobolev, S.V., Nikokosian, I.K. (2005) An olivine-free
1404 mantle source of Hawaiian shield basalts. *Nature* **434**, 590-597.
1405
- 1406 Sobolev, A.V., Hofmann, A.W., Kuzmin, D.V., Yaxley, G.M., Arndt, N.T., Chung, S.-L.,
1407 Danyushevsky, L.V., Elliott, T., Frey, F.A., Garcia, M.O., Gurenko, A.A., Kamenetsky,
1408 V.S., Kerr, A.C., Krivolutsкая, N.A., Matvienkov, V.V., Nikogosian, I.K., Rocholl, A.,
1409 Sigurdsson, I.A., Sushchevskaya, N.M., Teklay, M. (2007) The amount of recycled crust
1410 in mantle-derived melts. *Science* **316**, 412-417.
1411
- 1412 Stern, C.R., Saul, S., Skewes, M.A., Futa, K. (1989) Garnet peridotite xenoliths from the
1413 Pali-Aike alkali basalts of southern-most South America. In: *Kimberlites and related*
1414 *rocks*, (Ed: Ross, J.) *Geol. Soc. Austral. Spec. Publ.* **14**. Blackwell, Perth. Vol 2, 735-744.
1415
- 1416 Stosch H.G., Seck H.A. (1980) Geochemistry and mineralogy of two spinel peridotite suites
1417 from Dreiser Weiher, West Germany. *Geochim. Cosmochim. Acta* **44**, 457-470.

1418

1419 Stracke, A., Hofmann, A.W., Hart, S.R. (2005) FOZO, HIMU and the rest of the mantle zoo.

1420 *Geochem., Geophys., Geosys.* **6**, doi:10.1029/2004GC000824.

1421

1422 Sun, W., Bennett, V.C., Kamenetsky, V.S. (2004) The mechanism of Re enrichment in arc

1423 lavas: evidence from Lau basin basaltic glasses and primitive melt inclusions. *Earth*

1424 *Planet. Sci. Lett.* **222**, 101-114.

1425

1426 Tarantola A., Valette B. (1982) Generalized non-linear inverse problems solved using the

1427 least squares criterion. *Rev. Geophys. Space Phys.* **20**, 219–232.

1428

1429 Thompson, R.N., Ottley, C.J., Smith, P.M., Pearson, D.G., Dickin, A.P., Morrison, M.A.,

1430 Leat, P.T., Gibson, S.A. (2005) Source of the Quaternary alkalic basalts, picrites and

1431 basanites of the Potrillo volcanic field, New Mexico, USA: Lithosphere or convecting

1432 mantle? *J.Petrol.* **46**, 1603-1643.

1433

1434 van Acken, D., Becker, H., Walker, R.J., McDonough, W.F., Wombacher, F., Ash, R.D.,

1435 Piccoli, P.M. (2010) Formation of pyroxenite layers in the Totalp ultramafic massif (Swiss

1436 Alps) - Insights from highly siderophile elements and Os isotopes. *Geochimica et*

1437 *Cosmochimica Acta* **74**, 661-683.

1438

1439 Volkening J., Walczyk T., Heumann K. (1991) Os isotope ratio determinations by negative

1440 thermal ionisation mass spectrometry. *Int. J. Mass Spectrom. Ion Process.* **105**, 147–159.

1441

1442 Walker, R.J, Morgan J.W. (1989) Rhenium-osmium isotope systematics of carbonaceous

1443 chondrites. *Science* **243**, 519–22.

1444

1445 Wang, K.L., O'Reilly, S.Y., Griffin, W.F., Pearson, N.J., Zhang, M. (2009) Sulphides in
 1446 peridotite xenoliths from Penghu Islands, Taiwan: melt percolation, PGE fractionation and
 1447 the lithospheric evolution of the South China block. *Geochim. Cosmochim. Acta* **73**, 4531-
 1448 4557.

1449

1450 Widom, E., Hoernle, K.A., Shirey, S.B., Schminke, H.-U. (1999) Os isotope systematics in
 1451 the Canary Islands and Madeira: lithospheric contamination and mantle plume signatures.
 1452 *J. Petrol.* **40**, 279-296.

1453

1454 Wilshire, H.G., Shervais, J.W. (1975) Al-augite and Cr-diopside ultramafic xenoliths in
 1455 basaltic rocks from the Western United States. *Phys. Chem. Earth* **9**, 257–272.

1456

1457 Wittig, N., Pearson, D.G., Baker, J.A., Duggen, S., Hoernle, K. (2010) A major element, PGE
 1458 and Re-Os isotope study of Middle Atlas (Morocco) peridotite xenoliths: Evidence for
 1459 coupled introduction of metasomatic sulphides and clinopyroxene. *Lithos* **115**, 15-26.

1460

1461 Workman, R.K., Hart, S.R., Jackson, M.G., Regelous, M., Farley, K.A., Blusztajn, J., Kurz,
 1462 M.D., Staudigel, H. (2004) Recycled metasomatized lithosphere as the origin of the
 1463 enriched mantle II (EM2) end-member: evidence from the Samoan volcanic chain.
 1464 *Geochem. Geophys. Geosys.* **5**, (2003GC000623).

1465

1466 Yaxley, G.M., Green, D.H. (1998) Reactions between eclogite and peridotite: mantle
 1467 refertilisation by subduction of oceanic crust. *Schweiz Mineral. Petrog. Mitt.* **78**, 243.

1468

1469 Zindler, A., Hart, S.R. (1986) Chemical geodynamics. *Ann. Rev. Earth Planet. Sci.* **14**, 493-

1470 571.

1471

1472

1473

1474

1475

1476

1477

1478

1479

1480

1481

1482

1483

1484

1485

1486

1487

1488

1489

FIGURE CAPTIONS

Figure 1. Rhenium and osmium elemental abundances of 28 spinel lherzolite xenoliths from Kilbourne Hole (this study) and similar samples from the same locality (Morgan, 1986; Burton et al., 1999; Meisel et al., 2001). All concentrations in parts per billion (ppb). Grey square illustrates estimates for [Os] and [Re] of the primitive upper mantle (PUM) of 3.9 ppb and 0.35 ppb respectively (Becker et al., 2006).

Figure 2. (a) Re-Os isotope evolution diagram for the 28 bulk-rock peridotites from this study (Burton et al., 1999 and Meisel et al., 2001 shown for comparison). Scatter between $^{187}\text{Re}/^{188}\text{Os}$ and $^{187}\text{Os}/^{188}\text{Os}$ is particularly high amongst the xenoliths from Kilbourne Hole. The best fit line coincides with a calculated isochron age of 2.3 ± 0.7 Ga, but the relationship cannot be described as convincingly isochronous despite agreement with the ages derived from Sr isotope ratios of Roden et al. (1988) of $2.5 \text{ Ga} \pm 0.2 \text{ Ga}$. (b) “Aluminachron” diagram for same samples as (a). Using an immobile melt depletion index, e.g. bulk-rock aluminium abundance reduces the amount of scatter seen in (a) suggesting a certain degree of Re-mobility. Best fit line of 2.4 Ga passes through composition of PUM (Meisel et al., 2001). Dashed lines – calculated Os isotope ratios for different mantle Re-depletion ages ($T_{\text{RD}} = 1/\lambda \times \ln \{[(^{187}\text{Os}/^{188}\text{Os}_{\text{chon}} - ^{187}\text{Os}/^{188}\text{Os}_{\text{sample}})/^{187}\text{Re}/^{188}\text{Os}_{\text{chon}}] + 1\}$) (Shirey & Walker, 1998).

Figure 3. Chondrite-normalized platinum-group element concentrations for 5 bulk-rock Kilbourne Hole peridotites (KH03-10, KH03-15, KH03-16, KH03-21 & KH03-24) and the host basalt (CI chondrite values from Horan et al., 2003). Uncertainties (2σ) calculated from long-term reproducibility of reference material GP13 and from external reproducibility of repeat measurements on separate aliquots of samples from this study.

1515

1516 Figure 4. Major element abundances of 57 sulfides (see Table 3). Two low-Cu populations
1517 (0.08 to 4.68 wt %), defined by either a high or low Fe:Ni ratio, are broadly equivalent to
1518 pentlandite rich and pentlandite poor monosulfide solid solution (MSS) sulfides (Luguet et
1519 al., 2003, 2004). A third population of sulfide, with higher Cu content, is analogous to
1520 chalcopyrite rich sulfides from previous studies (Dromgoole & Pasteris, 1987; Luguet et al.,
1521 2003, 2004). Host basalt sulfide from Burton et al. (1999).

1522

1523 Figure 5. (a) Bulk rock peridotite [Os] vs. bulk rock Os isotope ratios. (b) [Os] and
1524 $^{187}\text{Os}/^{188}\text{Os}$ of individual sulfides from KH03-15 (n = 7), KH03-16 (n = 7), KH03-21 (n =
1525 10), and KH03-24 (n = 8). Open circles denote interstitial sulfides, closed circles denote
1526 enclosed sulfides. Grey box denotes range of [Os] and $^{187}\text{Os}/^{188}\text{Os}$ in (a). As in cratonic
1527 mantle sulfides (e.g. Griffin et al., 2004), and other non-cratonic sulfides (e.g. Harvey et al.,
1528 2006; 2010) the most unradiogenic sulfides possess the greatest [Os]. (c) Sulfide [Re] vs.
1529 sulfide [Os] for 7 interstitial and 12 enclosed sulfides from (b). There is no statistically
1530 significant co-variation between these variables, however sulfides with high [Re] tend to
1531 possess low [Os] and c. 50% of the high-[Os] enclosed have lower [Re] than the interstitial
1532 population.

1533

1534 Figure 6. Osmium mass balance for Kilbourne Hole xenoliths. The silicate and oxide phases
1535 (olivine, orthopyroxene, clinopyroxene and spinel) account for less than 5 % of the whole
1536 rock Os budget. Sulfide dominates the Os budget of all of the samples due to exceptionally
1537 high sulfide / silicate partition coefficients for Os (e.g. Fleet et al 1991, 1996). At least two
1538 populations of sulfide exist, in approximately equal modal abundance not exceeding a total of
1539 0.03 modal% (cf. Luguet et al., 2003; 2004), but their respective contribution to the Os mass

balance are not equal. In all samples, enclosed sulfides account for the vast majority of Os while the contribution from interstitial sulfide, in the case of KH03-24, is insignificant, and in KH03-15 and KH03-21 account for 3.5 - 17.5 % respectively of the Os present. The relative contributions of the two sulfide populations in KH03-16 is less clear but is probably dominated by the enclosed population. The contribution of the interstitial component in KH03-16 is calculated to be less than 17.5 % of the total. Relative contributions to the osmium budget were calculated on the basis of the [Os] and $^{187}\text{Os}/^{188}\text{Os}$ of individual components and the bulk-rock rather than by point counting the two populations of sulfide, which are sparse in thin section.

Figure 7. ^{187}Re - ^{187}Os isotope systematics for all mineral components, interstitial and enclosed sulfides and host basalt from KH03-15, KH03-16, KH03-21 & KH03-24. With the exception of KH03-16, all samples show a strong similarity between the ^{187}Re - ^{187}Os systematics of enclosed sulfides and the respective bulk-rock. Although no high-[Os] sulfides with particularly unradiogenic ($^{187}\text{Os}/^{188}\text{Os} < 0.120$) were recovered from KH03-16 a high-[Os], unradiogenic component, i.e. enclosed sulfide, must be present in KH03-16 to complete the Os mass balance (see text & Figure 6).

Figure 8. A simple two-stage model for the generation of EM-basalt Os isotope signatures. Black squares denote Os elemental abundance and isotope signature of EM-basalts worldwide (Martin et al., 1994; Bennett et al., 1996; Hauri & Kurz, 1996; Hauri et al., 1996; Lassiter & Hauri, 1998; Widom et al., 1999; Brandon et al., 1999, 2007; Lassiter et al., 2000, 2004; Skovgaard et al., 2001; Eisele et al., 2002; Workmann et al., 2004; Gaffney et al., 2005; Jamaïs et al., 2008; Debaille et al., 2009; Ireland et al., 2009; Day et al., 2009; Class et al., 2009). Dataset generated using GEOROC and filtered for EM-basalts with [Os] ≥ 40 ppt

1565 to control for the effects of crustal contamination. White bar represents the range of melts
 1566 produced by melting only silicate components from a fertile mantle precursor ($^{187}\text{Os}/^{188}\text{Os} =$
 1567 0.130), [Os] controlled by abundances measured in handpicked silicate aggregates from this
 1568 study and their approximate modal abundance). $D_{\text{Os}}^{\text{olivine/melt}} = 0.51$ from Burton et al., (2002)
 1569 but also modelled for $D_{\text{Os}}^{\text{olivine/melt}}$ of up to an order of magnitude greater to account for the
 1570 full range of PGE $D^{\text{olivine/melt}}$ with decreasing oxygen fugacity of Brenan et al. (2003). The Os
 1571 elemental abundance and isotope systematics of EM-basalts worldwide can be accounted for
 1572 by the sequential addition of first interstitial sulfides (1) followed by a contribution from
 1573 formerly enclosed sulfides (2) as melt depletion in the source peridotite continues (see text).
 1574 White circles denote individual Kilbourne Hole sulfides (this study), light- and mid-grey
 1575 circles are non-cratonic peridotite-derived sulfides from the Mid-Atlantic Ridge and the
 1576 French Massif Central (Harvey et al., 2006; 2010 respectively) and black circles are cratonic
 1577 sulfides (e.g. Griffin et al., 2004; Aulbach et al., 2004; Marchesi et al., 2009).
 1578

1579 Figure 9. Correlation of paired IPGE and paired PPGE in peridotite, individual peridotite-
 1580 derived sulfides and basalt. Compositions normalized to CI-chondrite (Horan et al., 2003). (i)
 1581 Ir_N vs. Os_N for peridotites from this study (a), worldwide peridotites; inset = this study (b),
 1582 mantle derived sulfides (c), and worldwide basalts (d). (ii) Pd_N vs. Pt_N , (iii) Pt_N vs. Os_N . The
 1583 strong correlation of pairs of IPGE (i) and pairs of PPGE (ii), but lack of correlation between
 1584 IPGE/PPGE pairs (iii) suggests that the two groups behave independently during progressive
 1585 melt depletion. Key: (a) Yellow discs = this study (b) Yellow discs = this study; red discs =
 1586 Bene Boussera, dark brown discs = Lesotho, grey discs = Namibia, orange discs = Vitim
 1587 (Pearson et al., 2004); light blue discs = Oman ophiolite, (Hanghøj et al., 2010); purples discs
 1588 = Atlas, Morocco (Wittig et al., 2010); pink discs = Massif Central (Lorand et al., 2003). (c)
 1589 Pink discs = Massif Central (Lorand et al., 2003); Dark green discs = Slave Craton, Canada

(Aulbach et al., 2004); White discs = abyddal peridotite (Luguet et al., 2001, 2003, 2004). (d)
White discs = Kilauea basalts (Pitcher et al., 2009); dark grey discs = Guizhou, China (Qi &
Zhou, 2008); light grey discs = Hawaiian picrite (Ireland et al., 2010); black discs =
Philippines Sea (Dale et al., 2008). For interpretation of the references to colour in this figure
legend, the reader is referred to the web version of this article.

1615

1616

TABLES

Sample	Al ₂ O ₃ /SiO ₂	[Os]	[Re]	¹⁸⁷ Os/ ¹⁸⁸ Os	2 s.e.	¹⁸⁷ Re/ ¹⁸⁸ Os	T _{RD}
KH03-10(L) ^a	0.282	0.13	0.40	0.16961	0.00007	0.16963	b
KH03-2 ^c	0.063	1.39	0.04	0.12125	0.00013	0.12408	0.85
KH03-3 ^c	0.096	1.22	0.07	0.13391	0.00014	0.26948	b
KH03-4 ^c	0.086	2.02	0.07	0.12966	0.00016	0.14829	b
KH03-5 ^c	0.070	2.10	0.08	0.12723	0.00013	0.17084	b
KH03-6 ^c	0.072	1.54	0.06	0.12668	0.00017	0.18251	0.05
KH03-6 ^{ce}	-	1.60	0.08	0.12721	0.00026	0.24318	b
KH03-6 ^{ce}	-	1.48	0.06	0.12689	0.00010	0.18255	0.02
KH03-6 ^{ce}	-	1.52	0.06	0.12701	0.00016	0.17263	0.00
KH03-7 ^c	0.055	2.25	0.07	0.12260	0.00014	0.13757	0.65
KH03-10 ^c	0.072	3.36	0.19	0.12520	0.00013	0.26084	0.27
KH03-10 ^{de}	-	3.36	0.19	-	-	-	-
KH03-10 ^{de}	-	3.23	0.23	-	-	-	-
KH03-11 ^c	0.078	1.63	0.07	0.12570	0.00018	0.20013	0.19
KH03-12 ^c	0.078	1.92	0.10	0.12566	0.00026	0.22697	0.20
KH03-14 ^c	0.090	1.52	0.07	0.12911	0.00030	0.22039	b
KH03-15 ^c	0.027	2.01	0.02	0.12131	0.00016	0.04353	0.84
KH03-15 ^{de}	-	2.01	0.02	-	-	-	-
KH03-15 ^{de}	-	2.04	0.03	-	-	-	-
KH03-16 ^c	0.025	2.84	0.01	0.11600	0.00026	0.00872	1.62
KH03-16 ^{de}	-	2.96	0.002	-	-	-	-
KH03-16 ^{de}	-	3.04	0.01	-	-	-	-
KH03-17 ^c	0.079	1.83	0.07	0.12775	0.00013	0.17599	b
KH03-18 ^c	0.075	2.50	0.12	0.12627	0.00043	0.2138	0.11
KH03-18 ^{de}	-	2.40	0.16	-	-	-	-
KH03-18 ^{de}	-	2.50	0.12	-	-	-	-
KH03-21 ^c	0.097	1.72	0.13	0.13247	0.00011	0.30562	b
KH03-21 ^{ce}	-	1.71	0.07	0.13235	0.00012	0.18475	b
KH03-21 ^{ce}	-	1.79	0.06	0.13215	0.00027	0.15138	b
KH03-21 ^{de}	-	1.72	0.13	-	-	-	-
KH03-21 ^{de}	-	1.71	0.07	-	-	-	-
KH03-21 ^{de}	-	1.79	0.06	-	-	-	-
KH03-21 ^{de}	-	1.73	0.08	-	-	-	-
KH03-22 ^c	0.057	1.75	0.05	0.12137	0.00030	0.13257	0.83
KH03-23 ^c	0.076	1.59	0.07	0.12488	0.00011	0.19362	0.32
KH03-24 ^c	0.059	1.39	0.06	0.12334	0.00014	0.14757	0.54
KH03-24 ^{ce}	-	1.79	0.04	0.11919	0.00020	0.07685	1.16
KH03-24 ^{de}	-	1.39	0.06	-	-	-	-
KH03-24 ^{de}	-	1.39	0.05	-	-	-	-
KH03-25 ^c	0.050	1.73	0.02	0.11936	0.00015	0.05207	1.13
KH03-26 ^c	0.078	1.44	0.05	0.12687	0.00012	0.16681	0.02
KH03-27 ^c	0.030	1.54	0.03	0.12031	0.00356	0.08833	0.99

KH96-1 ^c	0.065	1.18	0.05	0.12411	0.00030	0.05244	0.43
KH96-2 ^c	0.041	1.16	0.03	0.11885	0.00013	0.12372	1.21
KH96-8 ^c	0.063	1.60	0.28	0.13090	0.00013	0.83201	^b
KH96-18 ^c	0.075	0.80	0.04	0.12936	0.00014	0.19627	^b
KH96-20 ^c	0.082	2.26	0.27	0.13268	0.00014	0.4895	^b
KH96-21 ^c	0.019	3.54	0.02	0.11588	0.00014	0.02138	1.64
KH96-24 ^c	0.059	2.39	0.68	0.12679	0.00014	1.35525	0.03

1617

1618 Table 1. Bulk-rock Al₂O₃/SiO₂, Re and Os elemental abundance and Re-Os isotope
1619 systematics of 28 peridotite xenoliths from Kilbourne Hole, New Mexico, USA. Al₂O₃/ SiO₂
1620 calculated from wt.% of oxides derived by XRF at The Open University. Major element data
1621 quality assessed using two rock standards (WS-E and OUG-94). Reproducibility is within 2%
1622 of recommended values. Complete major and trace element abundances for all of the samples
1623 are the subject of a separate contribution (Hammond et al., 2010). [Re] and [Os] expressed in
1624 parts per billion (ppb). Errors shown as 2σ mean. T_{RD} = (minimum) time of rhenium
1625 depletion calculated using a mean present-day chondritic value ¹⁸⁷Os/¹⁸⁸Os = 0.127 (Luck &
1626 Allègre, 1983; Walker & Morgan, 1989) and assumes that ¹⁸⁷Re/¹⁸⁸Os_{sample} = 0. Given isotope
1627 ratios blank corrected. ¹⁸⁷Os/¹⁸⁸Os ratios normalised to ¹⁹²Os/¹⁸⁸Os = 3.08271 and corrected
1628 using measured ¹⁸O/¹⁶O and ¹⁷O/¹⁶O of 0.002047 and 0.00037, respectively. Johnson Matthey
1629 (n = 26) 2.75 ng Os standard ¹⁸⁷Os/¹⁸⁸Os = 0.17373 ± 12 (2σ). ^a host lava. ^b “future” age. ^c
1630 Carius tube digestion. ^d high pressure asher digestion for PGE concentration measurement.
1631 For all PGE abundances please refer to Table 4. ^e duplicate measurement.

1632

1633

1634

1635

1636

1637

1638

1639

Sample	[Os]	[Re]	$^{187}\text{Os}/^{188}\text{Os}$	2 s.e.	$^{187}\text{Re}/^{188}\text{Os}$
KH03-15 olivine	36.0	24.4	0.1232	0.0007	5.11
KH03-15 opx	45.9	36.8	0.1315	0.0018	6.08
KH03-15 cpx	420	37.4	0.1250	0.0009	0.68
KH03-15 spinel	1633	47.1	0.1215	0.0005	0.22
KH03-16 olivine	10.4	22.0	0.1238	0.0022	10.0
KH03-16 opx	142	53.4	0.1201	0.0008	0.26
KH03-16 cpx	2620	535.8	0.1167	0.0003	0.97
KH03-16 spinel	805	520.2	0.1307	0.0017	3.35
KH03-21 olivine	33.6	2.84	0.1309	0.0006	0.63
KH03-21 opx	38.2	152	0.1328	0.0011	30.1
KH03-21 cpx	63.8	85.7	0.1391	0.0016	10.2
KH03-21 spinel	1630	167	0.1525	0.002	0.78
KH03-24 olivine	26.9	12.2	0.1299	0.0014	3.62
KH03-24 opx	33.7	10.4	0.1324	0.0009	2.35
KH03-24 cpx	65.1	89.1	0.1617	0.0003	10.4
KH03-24 spinel	826	818	0.1245	0.0007	7.51

1640

1641 Table 2. Re–Os isotope data for mineral separates from KH03-15, KH03-16, KH03-21 &
 1642 KH03-24. Errors shown are 2 σ mean. Re and Os concentrations expressed as parts per trillion
 1643 (ppt). Standards and corrections for $^{18}\text{O}/^{16}\text{O}$ and $^{17}\text{O}/^{16}\text{O}$ as in Table 1.

1644

1645

1646

1647

1648

1649

1650

1651

1652

1653

1654

Sample	Ni	Cu	S	Fe	Co	Zn	Si	Total
KH03-11_A1	16.03	0.61	36.69	45.34	0.31	0.00	0.03	99.00
KH03-11_A1	34.14	1.31	33.20	31.15	0.46	0.00	0.01	100.27
KH03-14_A10	16.02	0.78	37.48	44.28	0.31	0.00	0.00	98.87
KH03-14_A10	8.89	4.44	37.16	48.88	0.23	0.00	0.00	99.61
KH03-14_A10	1.74	20.99	34.81	40.17	0.14	0.02	0.00	97.86
KH03-14_A9	15.03	0.63	37.35	45.50	0.31	0.00	0.00	98.83
KH03-14_A8	17.71	0.44	36.37	43.70	0.28	0.00	0.00	98.50
KH03-14_A8	11.40	11.69	35.25	39.97	0.19	0.01	0.00	98.51
KH03-14_A9	1.92	21.44	35.15	39.75	0.13	0.01	0.00	98.40
KH03-14_A7	19.50	4.56	35.08	35.84	0.36	0.02	1.15	96.50
KH03-14_A7	16.13	0.66	37.49	44.63	0.30	0.00	0.00	99.21
KH03-14_A6	13.30	0.44	37.24	47.52	0.26	0.00	0.00	98.76
KH03-14_A5	17.05	0.77	37.19	44.18	0.29	0.00	0.00	99.48
KH03-14_A4	15.76	0.73	37.50	45.33	0.30	0.00	0.00	99.63
KH03-14_A3	14.78	0.37	38.08	45.09	0.30	0.00	0.01	98.63
KH03-14_A2	14.66	0.55	37.64	45.99	0.31	0.01	0.00	99.16
KH03-14_A1	15.14	0.77	37.31	45.98	0.31	0.00	0.00	99.52
KH03-15_1.1	28.76	0.68	34.71	35.01	0.30	0.00	0.00	99.47
KH03-17_A1	23.26	0.23	37.93	38.17	0.29	0.00	0.00	99.87
KH03-17_A2	25.88	0.31	37.75	35.64	0.29	0.01	0.00	99.87
KH03-21_1.1	29.39	1.72	32.61	35.26	0.29	0.00	0.00	99.27
KH03-21_1.1	27.32	4.68	32.79	33.87	0.30	0.00	0.00	98.96
KH03-21_1.2	28.45	1.71	33.15	36.13	0.29	0.00	0.00	99.74
KH03-21_1.2	26.90	4.61	33.12	35.02	0.30	0.00	0.00	99.95
KH03-21_1.3	31.95	1.84	32.41	31.81	0.33	0.00	0.00	98.34
KH03-21_1.3	8.79	0.12	37.50	51.19	0.17	0.00	0.00	97.78
KH03-21_2.1	16.27	0.28	37.32	45.54	0.32	0.01	0.00	99.74
KH03-21_2.2	23.86	0.20	37.12	38.23	0.28	0.02	0.00	99.71
KH03-21_2.2	2.69	22.59	34.17	38.63	0.09	0.00	0.00	98.17
KH03-21_3.1	16.26	0.51	36.61	44.66	0.32	0.00	0.00	98.36
KH03-21_3.2	28.27	2.23	32.06	34.91	0.30	0.00	0.08	97.85
KH03-21_3.2	21.26	9.25	32.34	35.15	0.24	0.00	0.00	98.24

KH03-21_4.1	10.86	0.53	36.61	51.03	0.29	0.00	0.02	99.34
KH03-21_4.1	28.43	0.32	33.99	37.41	0.63	0.00	0.00	100.77
KH03-22_A1	34.08	1.64	33.00	30.58	0.25	0.00	0.02	99.56
KH03-22_A3	17.17	0.62	37.28	44.37	0.27	0.00	0.00	99.71
KH03-22_A3	33.46	1.65	33.16	31.20	0.29	0.00	0.02	99.79
KH03-22_A3	29.88	4.26	34.10	32.16	0.28	0.00	0.00	100.68
KH03-22_A4	34.77	1.21	32.31	30.09	0.28	0.00	0.20	98.85
KH03-22_A4	17.75	0.39	37.76	43.64	0.28	0.00	0.00	99.81
KH03-22_A5	19.17	0.45	37.84	41.91	0.24	0.00	0.00	99.62
KH03-22_A5	36.16	0.95	33.10	28.58	0.29	0.00	0.09	99.17
KH03-22_A6	18.69	0.49	37.39	42.94	0.24	0.00	0.00	99.75
KH03-22_B1.1	14.38	0.32	37.28	45.47	0.20	0.00	0.00	97.65
KH03-22_B1.2	28.23	0.47	34.70	36.35	0.30	0.00	0.03	100.07
KH03-22_B1.3	16.13	0.30	38.29	44.18	0.25	0.00	0.06	99.22
KH03-22_B1.4	31.54	2.12	33.18	30.75	0.32	0.00	0.19	98.09
KH03-22_B1.4	12.55	0.41	38.17	48.15	0.23	0.02	0.03	99.57
KH03-22_B2	19.65	0.54	36.18	40.99	0.24	0.01	0.01	97.63
KH03-22_B3.1	31.93	1.59	33.02	31.86	0.32	0.00	0.02	98.74
KH03-22_B3.1	13.09	0.55	37.36	47.66	0.22	0.00	0.00	98.89
KH03-22_B3.2	34.07	1.11	32.71	30.02	0.30	0.00	0.00	98.21
KH03-22_B3.2	17.56	0.23	37.25	43.34	0.24	0.00	0.00	98.62
KH03-22_B4.2	16.95	0.46	36.98	43.82	0.27	0.01	0.07	98.57
KH03-22_B4.1	32.71	1.00	33.49	30.94	0.29	0.00	0.00	98.42
KH03-22_B4.1	19.94	0.56	37.44	40.68	0.28	0.00	0.00	98.91
KH03-23_A1	1.10	25.91	34.21	36.11	0.04	0.01	0.01	97.39

1655

1656 Table 3. Major element abundances of sulfide grains in peridotite xenoliths from Kilbourne Hole,
1657 New Mexico, USA. Repeat analyses of an in-house pentlandite standard yields errors on major
1658 elements (S, Fe, Ni) of 2, 5 and 6 % (2 σ) respectively, with minor elements (Co, Cu) errors (2 σ)
1659 of 22% and 70% respectively.

1660

1661

1662

1663

	Sample	[Os]	2sd	[Ir]	+/-	[Ru]	+/-	[Pt]	+/-	[Pd]	+/-	[Re]	2sd
1664	KH03-10(L) ^a	0.13	0.01	0.14	0.01	0.31	0.02	0.48	0.19	0.61	0.24	0.40	0.16
1665	KH03-10	3.36		4.19	0.25	7.47	0.45	6.58	2.63	5.58	2.23	0.19	
1666	KH03-10 ^b	3.23										0.26	
	<i>mean</i>	<i>3.30</i>	<i>0.18</i>									<i>0.23</i>	<i>0.11</i>
1667	KH03-15	2.01		3.07	0.18	5.43	0.33	4.31	1.73	1.26	0.50	0.02	
1668	KH03-15 ^b	2.04										0.03	
	<i>mean</i>	<i>2.02</i>	<i>0.04</i>									<i>0.02</i>	<i>0.01</i>
1669	KH03-16	2.84		3.04	0.18	4.77	0.29	3.35	1.34	0.55	0.22	0.007	
	KH03-16 ^b	2.96										0.002	
1670	<i>mean</i>	<i>2.90</i>	<i>0.18</i>									<i>0.004</i>	<i>0.008</i>
1671	KH03-18	2.50		3.44	0.21	6.21	0.37	6.12	2.45	4.55	1.82	0.12	
	KH03-18 ^b	2.40										0.16	
1672	<i>mean</i>	<i>2.45</i>	<i>0.14</i>									<i>0.14</i>	<i>0.06</i>
	KH03-21	1.72		2.81	0.17	5.25	0.31	4.56	1.82	2.74	1.10	0.13	
1673	KH03-21 ^b	1.71										0.07	
1674	KH03-21 ^b	1.79										0.06	
	KH03-21 ^b	1.73										0.08	
1675	<i>mean</i>	<i>1.74</i>	<i>0.09</i>									<i>0.08</i>	<i>0.03</i>
1676	KH03-24	1.39		2.84	0.00	5.14	0.00	4.66	1.86	2.59	1.04	0.06	
	KH03-24 ^b	1.39										0.05	
1677	<i>mean</i>	<i>1.39</i>	<i>0.00</i>									<i>0.05</i>	<i>0.02</i>
1678													
1679													

Table 4. Platinum group element (+ Re) abundances in bulk-rock Kilbourne Hole peridotite xenoliths and host basalt. All concentrations shown in parts per billion (ppb). Precision of [Ir] & [Ru] measurements ($\pm 6\%$) calculated from the external reproducibility of [Os] on multiple measurements on several powder splits from each xenolith. Precision of [Pd] & [Pt] ($\pm 40\%$) calculated from the external reproducibility of [Re]. Internal, i.e. within-run precision is more than an order of magnitude better than external precision which is therefore the limiting factor on PGE concentration reproducibility in these samples. ^a host lava. ^b duplicate measurement by Carius tube digestion (or some HPA?).

Sample	Morphology	[Os]	[Re]	$^{187}\text{Os}/^{188}\text{Os}$	2 s.e.	$^{187}\text{Re}/^{188}\text{Os}$
KH03-15_2	interstitial	0.001	0.848	0.2163	0.0073	3575
KH03-15_4	enclosed	24.70	11.3	0.1195	0.0003	2.18
KH03-15_5	enclosed	36.9	2.83	0.1208	0.0002	0.37
KH03-15_6	enclosed	10.9	0.140	0.1202	0.0002	0.03
KH03-15_7	interstitial	6.05	-	0.1304	0.0003	-
KH03-15_9	enclosed	5.82	-	0.1185	0.0003	-
KH03-15_10	interstitial	21.2	-	0.1312	0.0004	-
KH03-16_2	interstitial	0.51	1.35	0.1349	0.0015	12.7
KH03-16_3	interstitial	0.010	138.9	0.1424	0.0050	68722
KH03-16_4	interstitial	1.48	34.27	0.1556	0.0051	111
KH03-16_5	enclosed	12.9	0.294	0.1235	0.0001	0.11
KH03-16_6	interstitial	0.024	3.133	0.1819	0.0057	622
KH03-16_9	interstitial	1.74	-	0.1362	0.0010	-
KH03-16_10	interstitial	0.052	-	0.3729	0.0169	-
KH03-21_1	interstitial	0.992	1.252	0.1303	0.0006	6.02
KH03-21_2	interstitial	1.11	1.181	0.1694	0.0004	5.11
KH03-21_3	enclosed	2.72	0.056	0.1283	0.0003	0.098
KH03-21_4	interstitial	10.0	23.32	0.1291	0.0001	101
KH03-21_5	enclosed	9.97	-	0.1259	0.0008	-
KH03-21_6	interstitial	1.29	-	0.1302	0.0008	-
KH03-21_7	interstitial	0.843	-	0.1368	0.0008	-
KH03-21_8	enclosed	4.48	-	0.1282	0.0005	-
KH03-21_9	interstitial	0.447	-	0.1764	0.0012	-
KH03-21_10	interstitial	0.584	-	0.1385	0.0005	-
KH03-24_5	enclosed	1.69	0.01	0.1227	0.0004	0.020
KH03-24_10	enclosed	0.195	0.002	0.1237	0.0028	0.050
KH03-24_11	enclosed	0.231	-	0.1240	0.0006	-
KH03-24_14	enclosed	2.76	0.04	0.1226	0.0013	0.070
KH03-24_15	enclosed	2.54	35.87	0.1234	0.0004	67.4
KH03-24_16	enclosed	2.50	18.78	0.1238	0.0011	35.8
KH03-24_17	interstitial	0.600	27.27	0.1264	0.0005	217
KH03-24_20	interstitial	0.314	-	0.1449	0.0017	-

1706

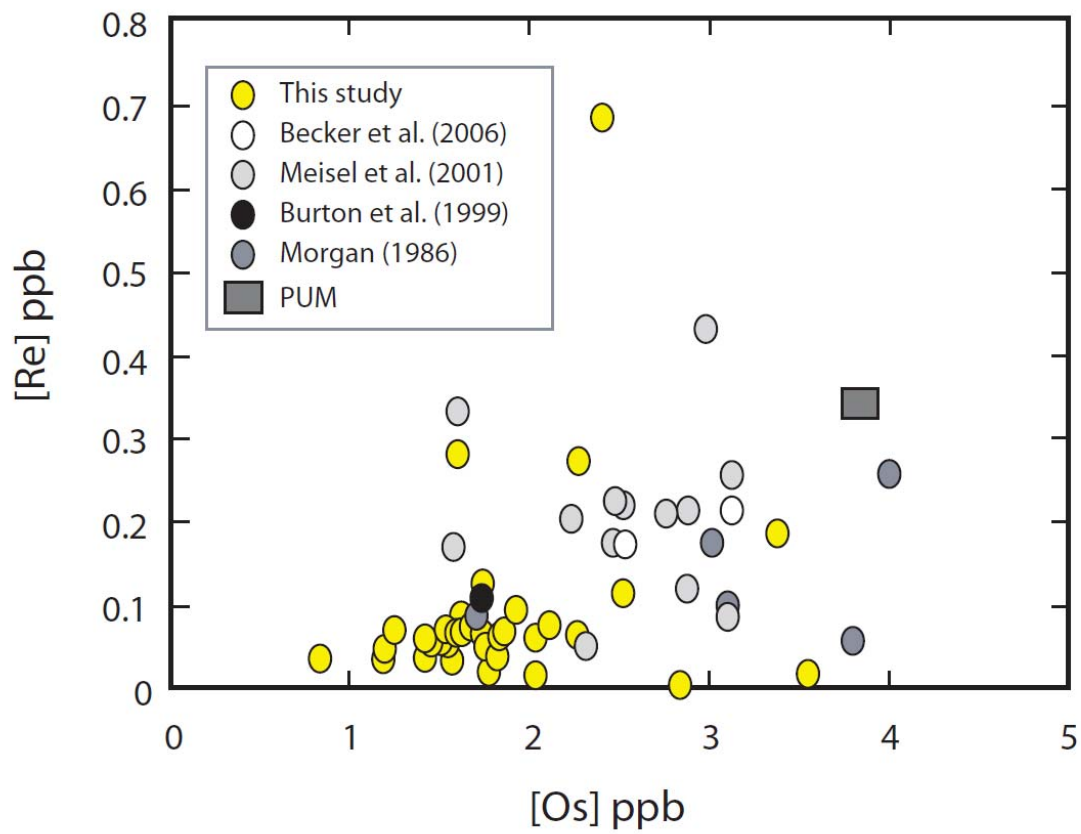
1707 Table 5. Re–Os elemental abundance and isotope data for sulfides from KH03-15, KH03-16,
1708 KH03-21 and KH03-24. Errors shown are 2 σ mean. Re and Os concentrations expressed as
1709 parts per million (ppm). Standards and corrections for $^{18}\text{O}/^{16}\text{O}$ and $^{17}\text{O}/^{16}\text{O}$ as in Table 2.

1710

1711

1712
1713
1714

FIGURES

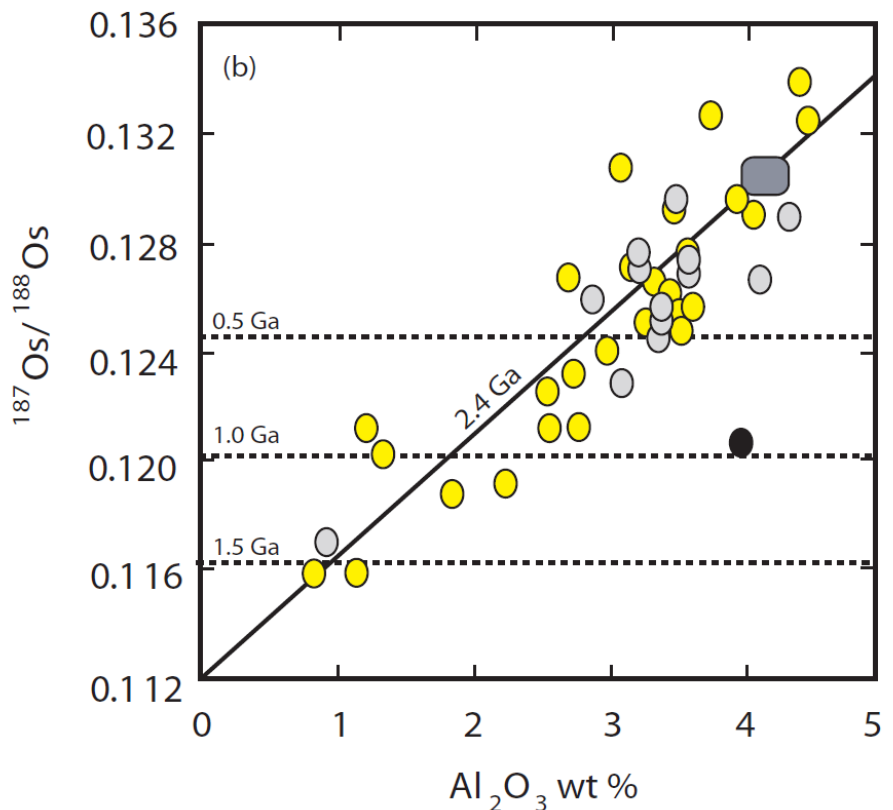
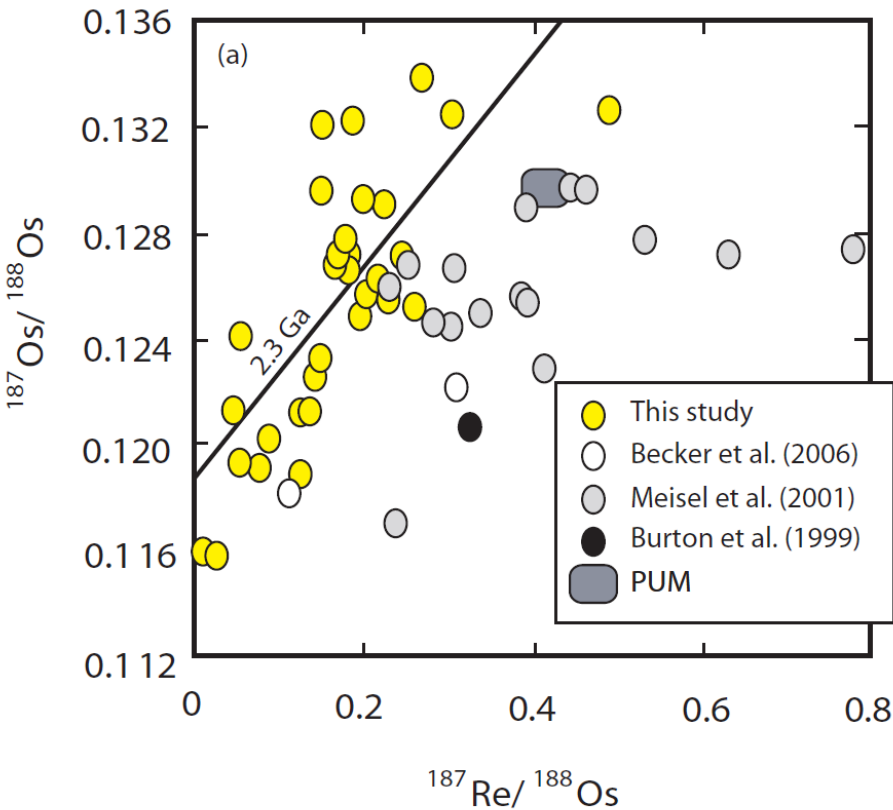


1715
1716 Figure 1

1717
1718
1719
1720
1721
1722
1723
1724
1725

1726

1727



1728

Figure 2

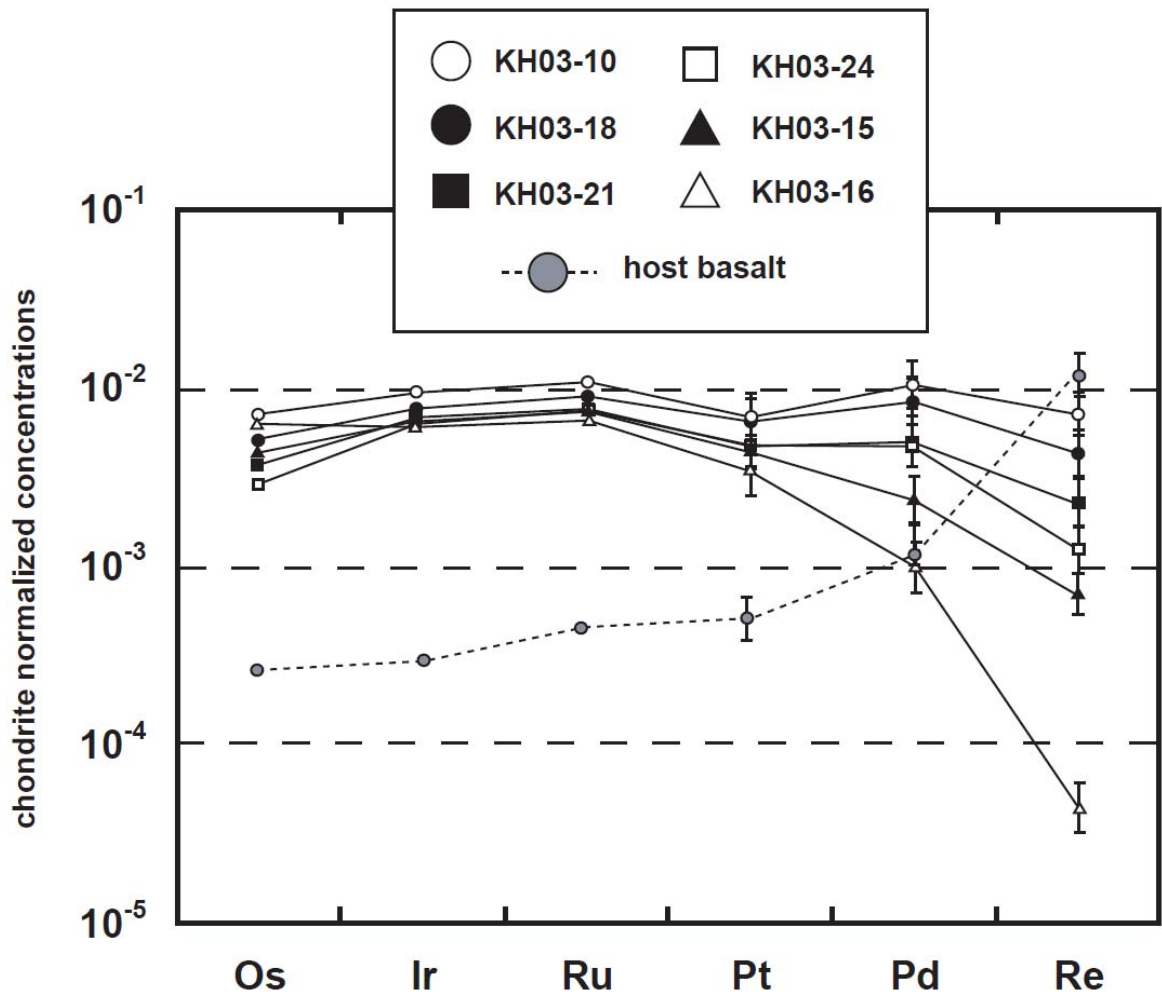
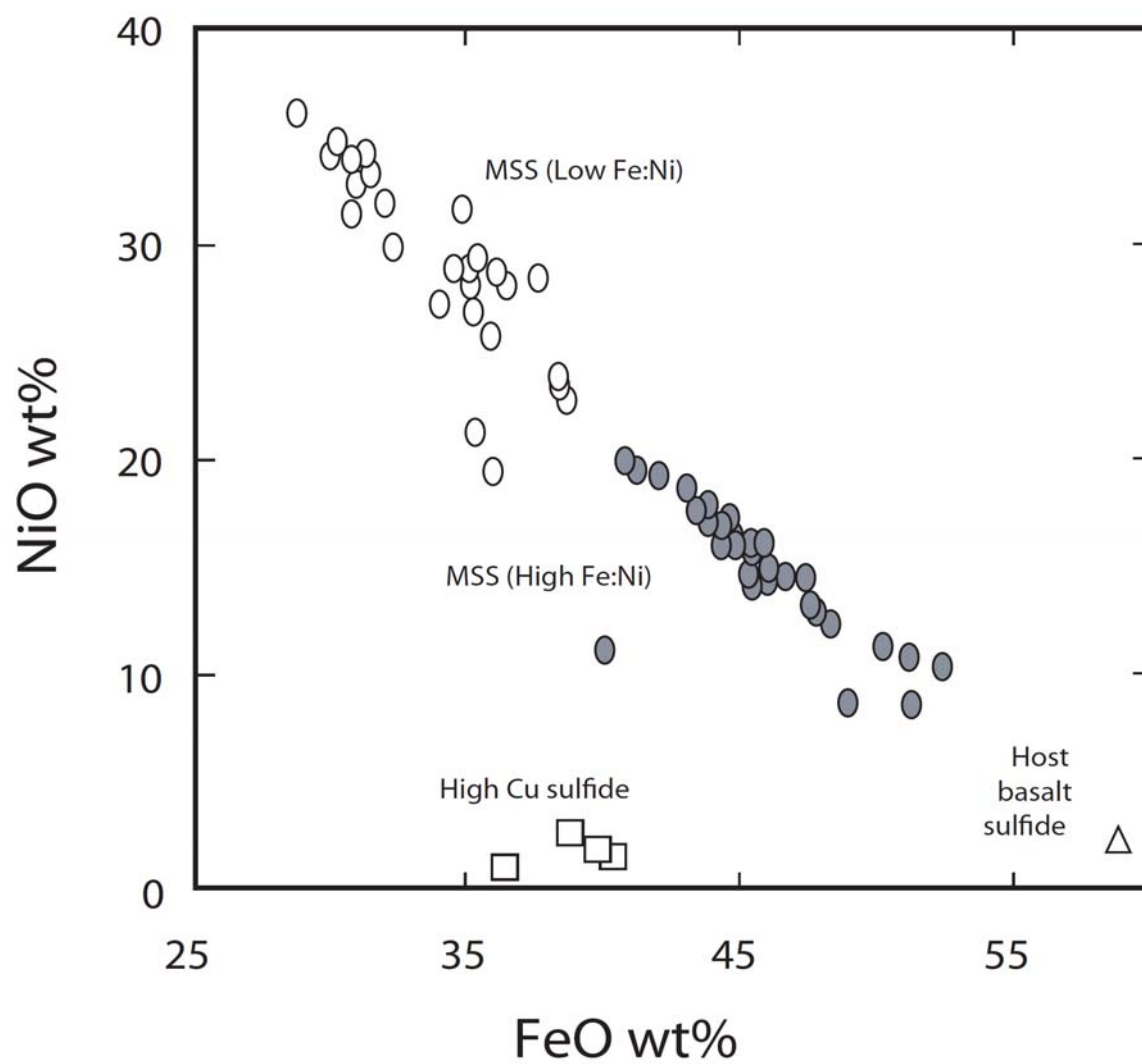


Figure 3

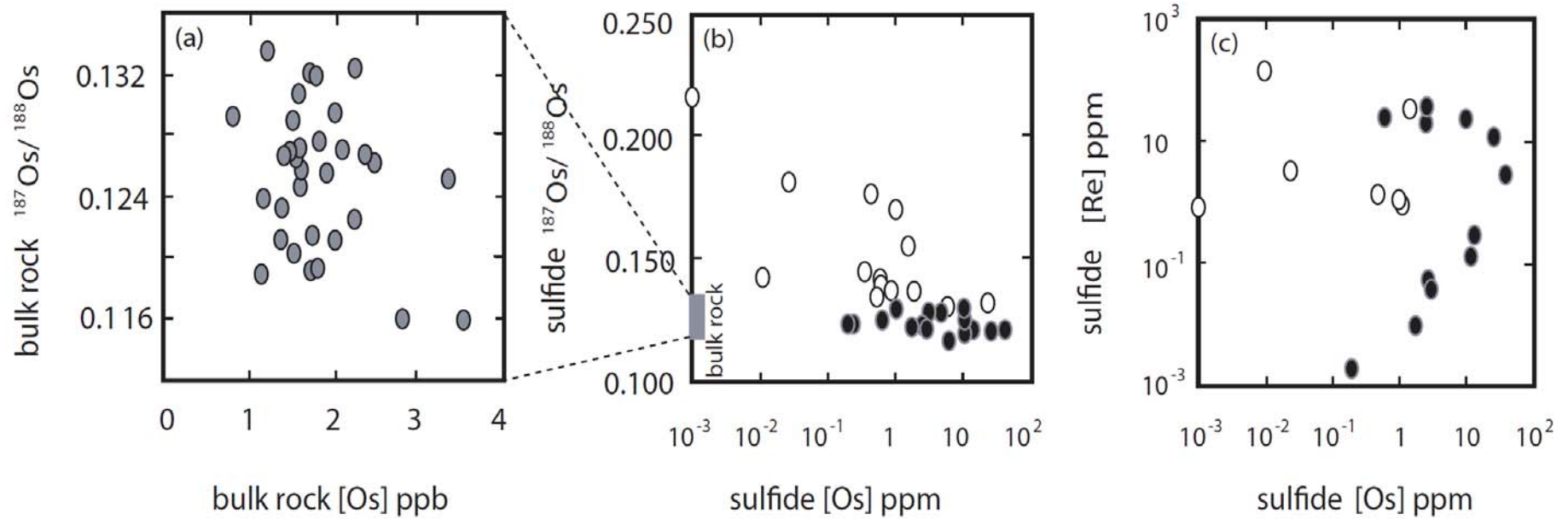
1741
1742



1743
1744 Figure 4

1745
1746
1747
1748
1749
1750
1751

1753



1754

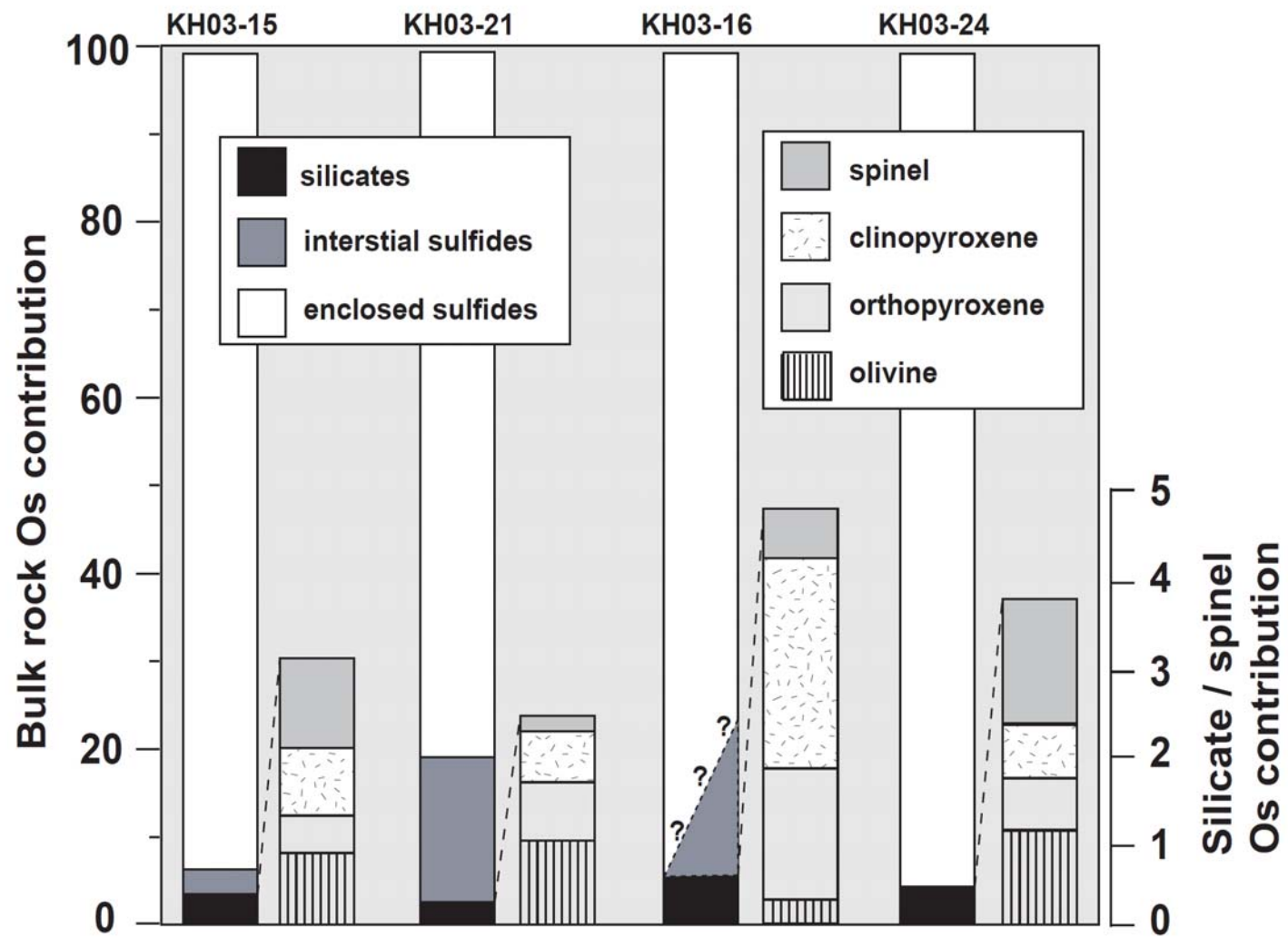
1755 Figure 5

1756

1757

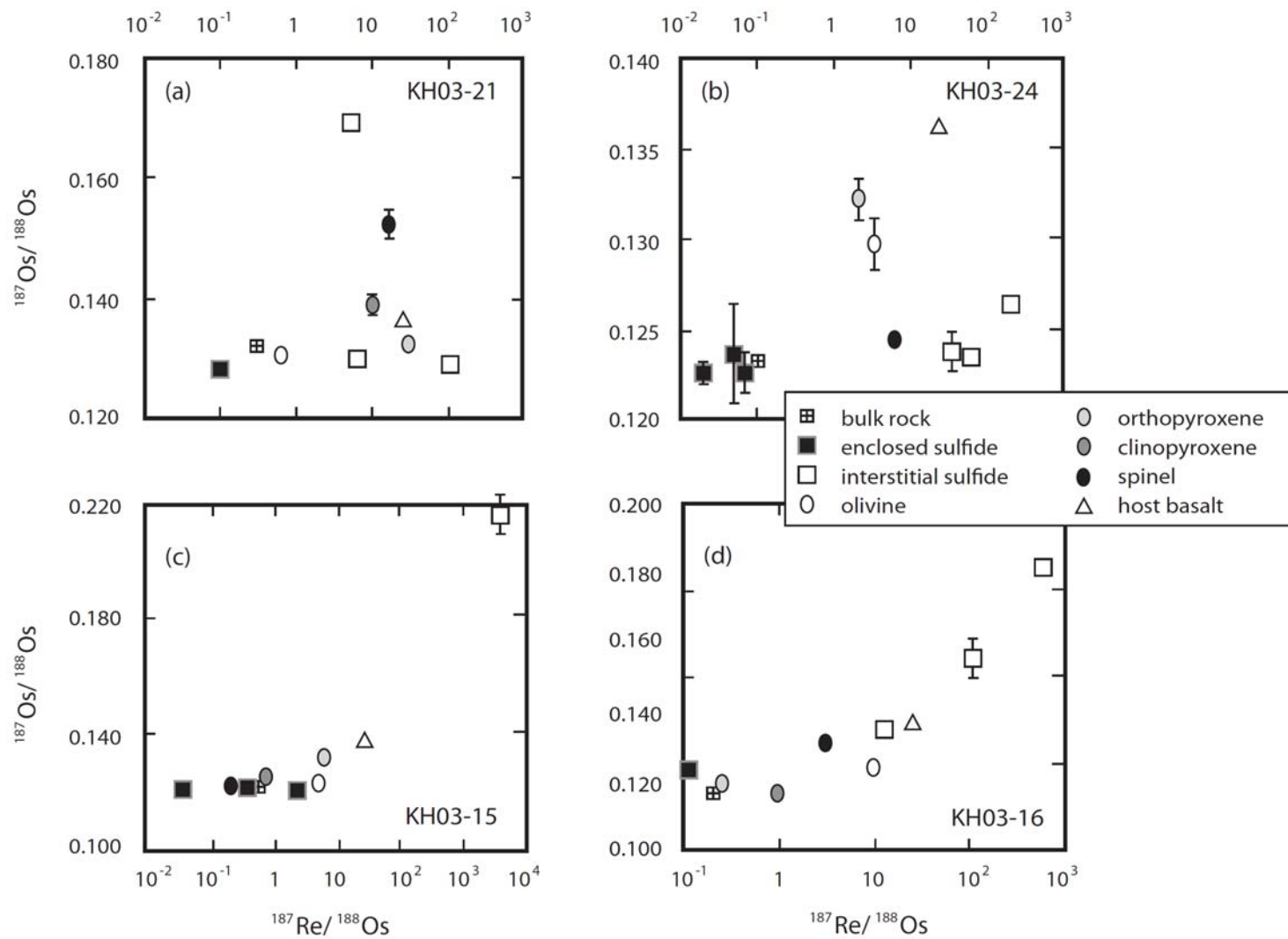
1758

1759



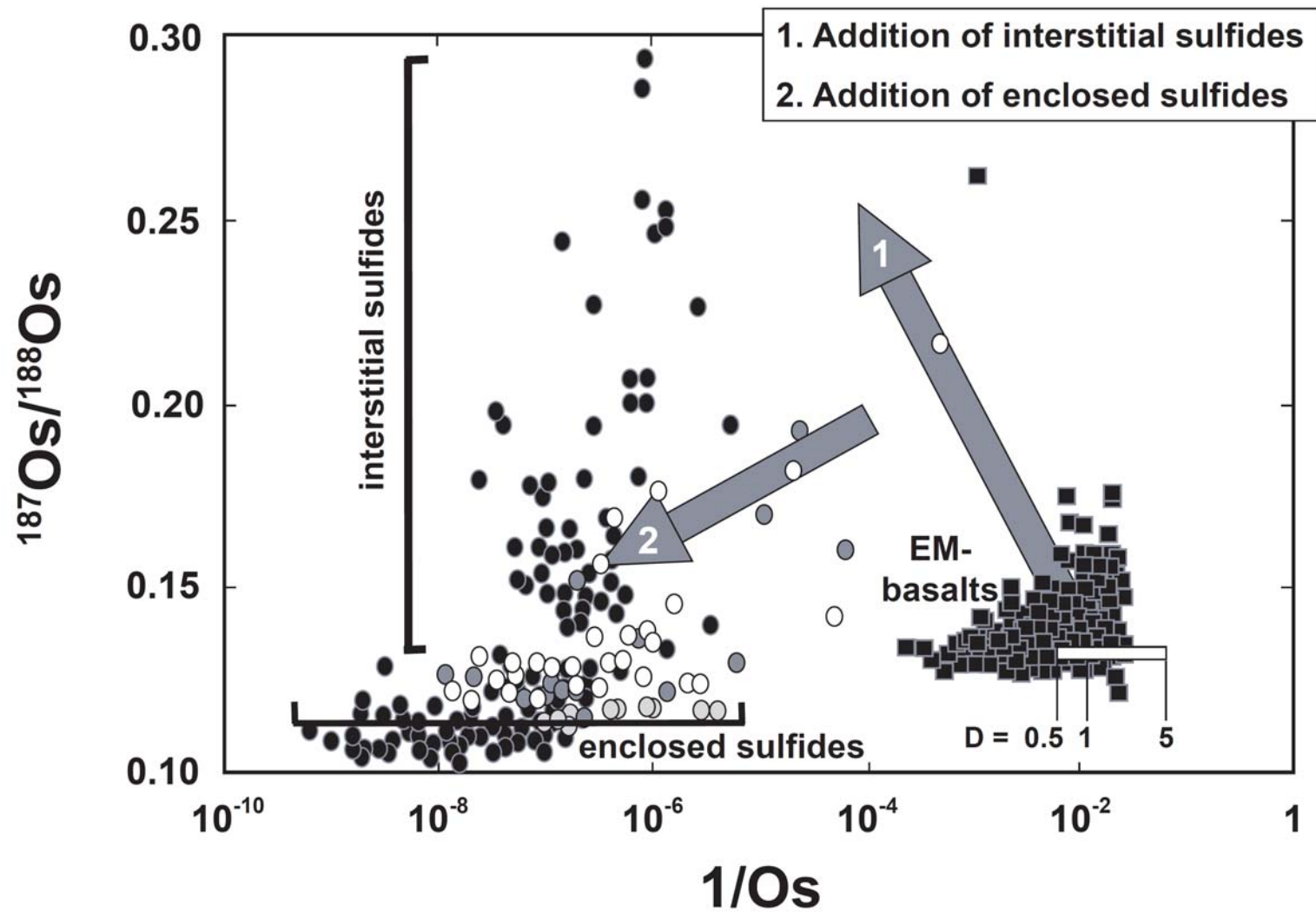
1760

1761 Figure 6



1762

1763 Figure 7



1764

1765 Figure 8

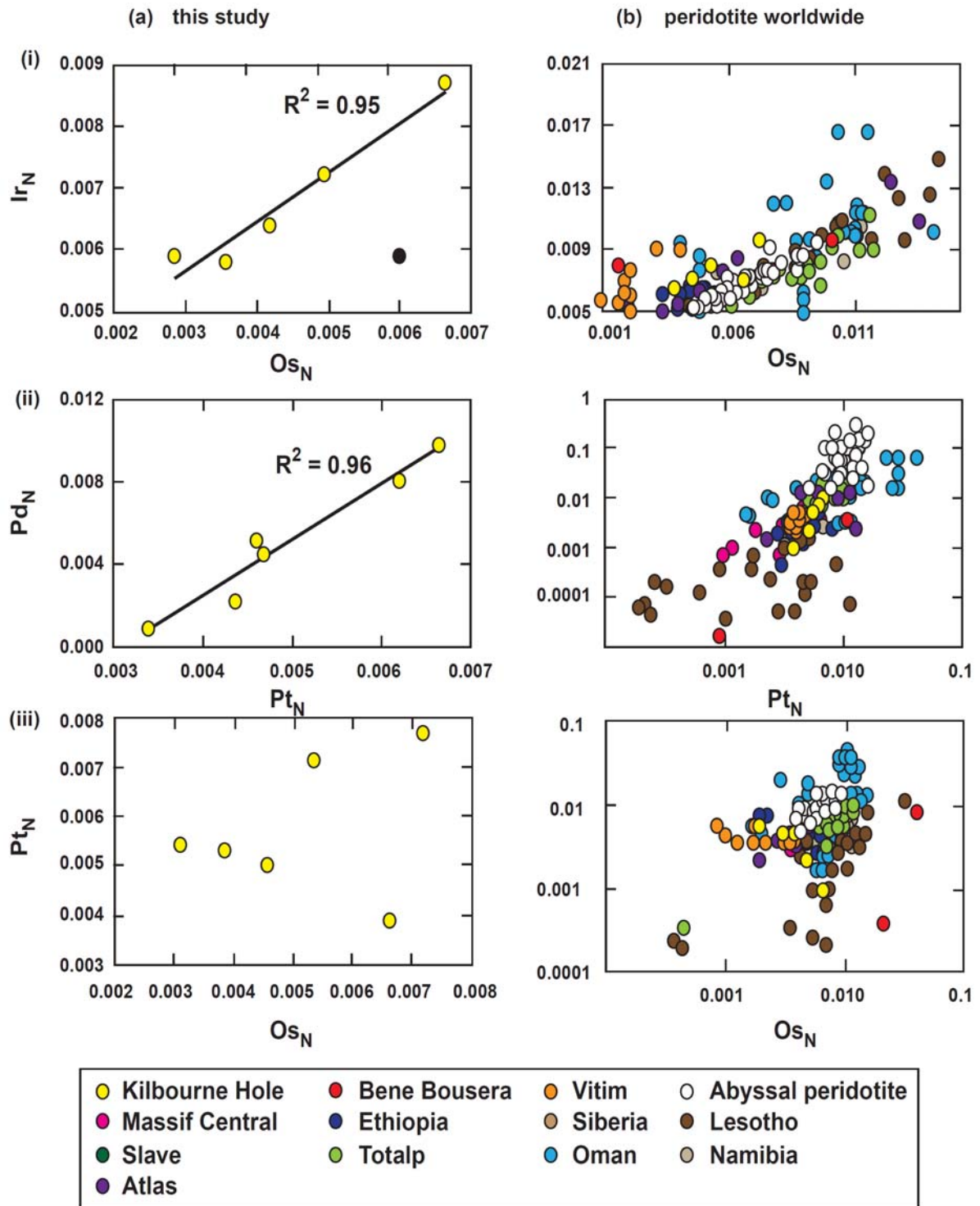
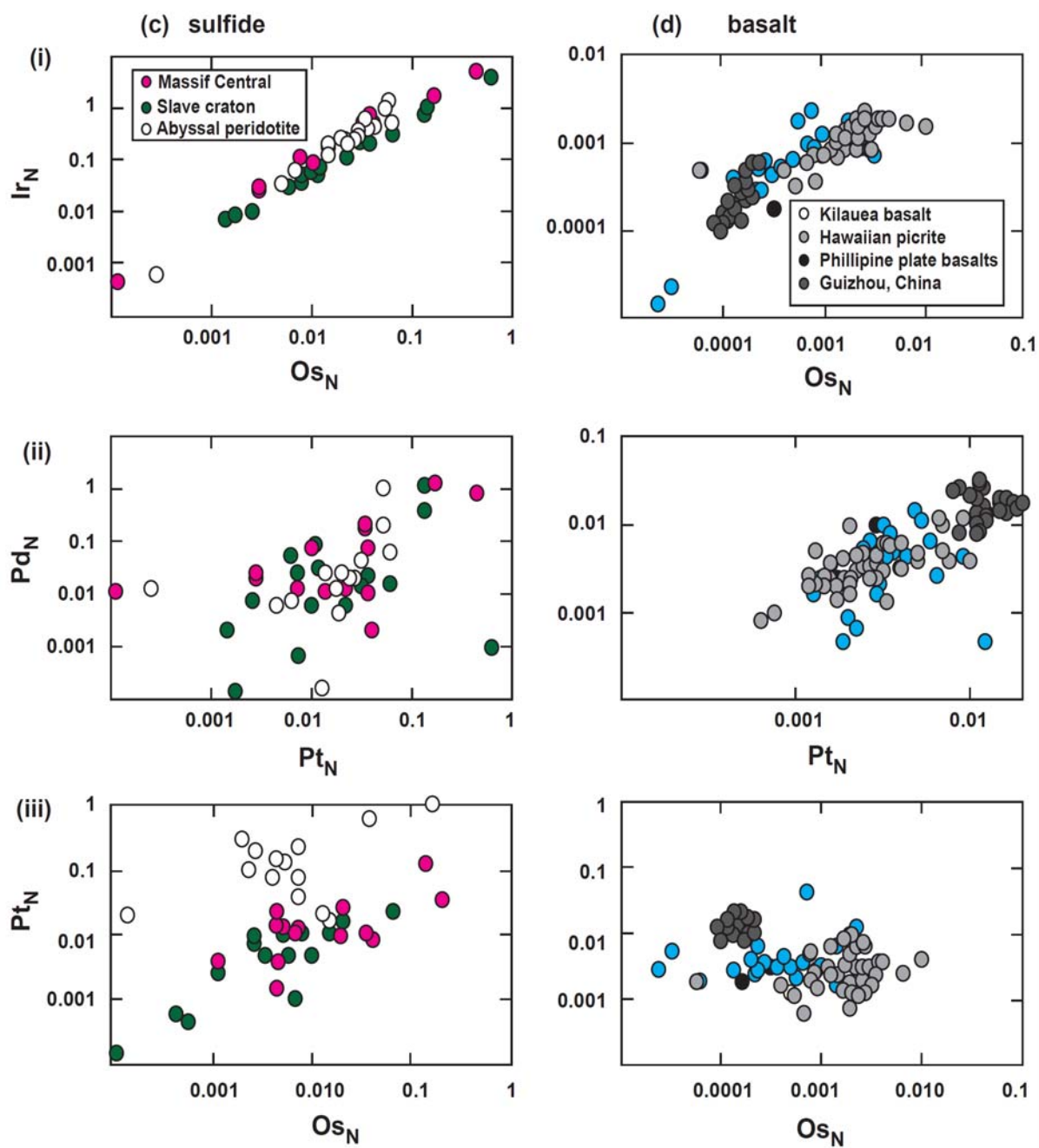


Figure 9 a



1771

1772 Figure 9 c & d